Composites: Part A 199 (2025) 109168

Contents lists available at ScienceDirect

Composites Part A

journal homepage: www.elsevier.com/locate/compositesa

Exploring the sustainability potential of lightweight structures made from *Phormium tenax* fibers by hybrid coreless filament winding

Pascal Mindermann [a,b,*], Yifan Lv [c,1], Malaya Prasad Behera [c,1], Romain Meot [d], Marie-Joo Le Guen [d], Sarat Singamneni [c]

[a] Cluster of Excellence Integrative Computational Design and Construction for Architecture (IntCDC), University of Stuttgart, Germany
[b] Institute for Textile and Fiber Technologies, University of Stuttgart, Germany
[c] Additive Manufacturing Research Center; School of Engineering, Computer and Mathematical Sciences; Auckland University of Technology, New Zealand
[d] Scion Group, New Zealand Institute for Bioeconomy Science Ltd, Rotorua, New Zealand

ARTICLE INFO

Dataset link: https://doi.org/10.18419/DARUS-5090

Keywords:
Coreless filament winding
Natural fibers
Phormium tenax
Linum usitatissimum

ABSTRACT

Fiber-reinforced plastics enable lightweight building systems through digitizable and automatable additive manufacturing techniques such as coreless filament winding (CFW). Replacing carbon fibers with low-CO_2-impact natural fibers offers opportunities for sustainable structures. A prior CFW study using four-point bending demonstrated the eco-mechanical potential of *Linum usitatissimum* fibers but was confined to simple sample geometries, emphasizing material over structural performance. This study addresses this limitation by introducing a new structural sample fabricated with a 3D-printed winding fixture and hybrid CFW. Samples from *Phormium tenax* fibers were experimentally benchmarked against carbon and *L. usitatissimum* fiber samples. Carbon samples exhibited 2.15× the mass/CO_2-specific stiffness and failure load of the natural fiber samples. *L. usitatissimum* slightly outperformed *P. tenax* due to greater raw material optimization. Projections suggest increasing fiber volume ratios, coupled with advances in fabrication, could close performance gaps while balancing lightweight and sustainability goals.

1. Introduction

The use of fiber composites in lightweight applications is advantageous primarily due to their high mass-specific mechanical properties. Furthermore, the anisotropic nature of these materials, along with the ability to adjust their composition, allows for tailoring of material properties to meet requirements of specific load cases. Although widely used in aerospace, fiber composites are also prominently employed in construction industry [1,2]. Fiber composite materials are often used as shell elements composed of multiple layers of woven textiles [3] or as lattice structures made from profiles [4]. Typically, profiles are produced by pultrusion [4], braiding [5], or filament winding [6]. Furthermore, robotic additive manufacturing techniques can create thermoplastic lattice structures with minimal support, offering greater design freedom compared to conventional 3D printing [7]. Beyond this palette of fabrication processes, coreless filament winding (CFW) [8–10] offers more design freedom at high mechanical performance as a fiber-based additive manufacturing technique where each bundle is placed individually suspended between points. CFW developed from conventional filament winding [11] by replacing the mold or mandrel by a winding fixture that drastically reduces contact area with the fiber composite to several point-like anchors [12]. If the contact area is only partially reduced, the process is referred to as hybrid CFW [13]. On the contrary, most recent CFW approaches increasingly avoid fixing the fibers by mutually interlocking fibers [14] or by implementing slack to the fiber net during fabrication [15]. In addition, CFW enables the creation of multi-material structures [16] and facilitates hybridization with other manufacturing processes [17]. Other advancements in CFW improve control over the fiber net by multi-stage winding [17] or over the fiber bundle cross-sectional shape by pultrusion-winding [18]. In construction applications, the winding fixture typically consists of clustered winding pins attached to a metal frame [12]. This introduced several advantages over conventional mold-based processes, notably the ease of reconfiguring structural components without significant investments in molds [19,20]. At an industrial scale, CFW is expected to be more cost-effective compared to conventional filament winding, as equipment investments (industrial robot or filament winding machine) and labor costs (operator and auxiliary personnel) are comparable depending on the specific implementation. However, CFW offers a higher

* Corresponding author at: Cluster of Excellence Integrative Computational Design and Construction for Architecture (IntCDC), University of Stuttgart, Germany.
E-mail address: pascal.mindermann@itft.uni-stuttgart.de (P. Mindermann).
[1] These authors contributed equally to this work.

https://doi.org/10.1016/j.compositesa.2025.109168
Received 12 April 2025; Received in revised form 3 July 2025; Accepted 6 July 2025
Available online 17 July 2025

degree of lightweighting, resulting in significant material savings, while winding fixtures are more affordable than molds and reusable across multiple projects. Although qualification costs may be higher due to the need for individualized components, they can be substantially reduced through modular design strategies. As in CFW, fibers are placed individually, each component can be fine-tuned, even without significant modifications to the fixture, by altering the sequence in which the fiber bundles are positioned on the winding anchors. This sequence defines the winding trajectory [21] and is referred to as winding syntax [22,23].

Current applications of (hybrid) CFW are increasingly seen in the production of lightweight truss structures [24,25]. However, challenges in CFW that require further investigation include reduced control over the composite material's composition and mesoscopic geometry. This limitation impacts the precision of FEA predictions, which are typically less accurate compared to other composite manufacturing processes [26,27]. As a result, full-scale failure tests are necessary to calibrate models, leading to the development of integrative design methods that span multiple disciplines [28,29]. Moreover, CFW faces productivity challenges as winding speeds are constrained by the online-impregnation capacity of the fabrication and material system. Even with pre-impregnated fibers, higher winding speeds increase the risk of fiber damage. Similar to other thermoset-based processes, throughput efficiency is further restricted by fixture occupation during matrix curing and the largely manual nature of pre- and post-processing steps. Beyond these challenges, CFW also has inherent limitations, such as inefficiency in producing structures with continuous surfaces or curved segments or segments with gradually varying thickness. Furthermore, the lack of established regulatory frameworks recognizing CFW in many applications presents an additional barrier to its broader adoption. In addition, in CFW fiber orientation and component geometry are coupled parameters in the design process, which is further complicated by the strong influence of fabrication parameters, such as fluctuating fiber tension, fiber–fiber interaction, local fiber volume ratio variations, and the lack of compaction during the consolidation. To address these uncertainties, current research efforts [30–32] aim to develop holistic digital representations of CFW structures. Based on this approach, an integrative co-design method [33] seeks to streamline design iterations by combining design/engineering methodologies, fabrication/construction processes, and material/building systems beyond disciplinary boundaries. This idea harnesses the full potential of digitization and automation within architecture, engineering, and construction (AEC) to increase productivity by gaining control over the entire production system.

Integrating sustainable fiber materials into CFW processes is another area of growing interest, especially in architectural applications [34,35], see Fig. 1. In fiber composites, substituting technical fibers, such as carbon or glass, with natural fibers, such as flax (*Linum*) or hemp (*Cannabis*), promises improvements in sustainability metrics but also entails adding further uncertainties and potential shortcomings [36,37]: The processing parameters for natural and technical fibers differ substantially due to the inherent characteristics of each material. Technical fibers, including fiber sizings, are highly engineered products that have undergone extensive optimization and tailored matrix systems to meet stringent performance criteria in specific applications. In contrast, commercially available natural fibers are often less optimized and still exhibit a range of processability and inconsistency challenges. Common issues [38,39] include inadequate wetting, undesirable hairiness, and hydrophilic properties. For natural fibers, the density is also depending on their moisture content [40]. Despite these challenges, natural fibers present several advantageous characteristics over technical fibers, such as lower density, better vibration damping, and enhanced thermal insulation properties, which are particularly attractive for occupant comfort in building applications. Furthermore, in terms of sustainability, natural fibers also offer a favorable environmental footprint. Their production generally requires less energy compared to the manufacturing of glass or carbon fibers, which involve energy-intensive processes like melting or high-temperature carbonization. In addition, natural fibers are biodegradable [41]. However, the environmental benefits of natural fibers must be balanced against their mechanical limitations and shorter lifecycles when used in load-bearing structures. Besides typically employed sustainability indicators such as global warming potential (GWP) and embodied energy a more holistic analysis [42] is advisable if a more detailed analysis is required. In CFW, energy-saving strategies should focus on raw material provision and for architectural applications also on component transportation, as energy savings from reduced component mass during the operational phase are neglectable [43]. Given the challenges of implementing effective recycling strategies for fiber composites, using renewable raw materials becomes increasingly important.

Fig. 1. Building system components made by coreless filament winding. Component made from predominantly European flax (*Linum usitatissimum*) fibers with epoxy resin (top) and similar building system incorporating a timber plate (bottom). Copyright by IntCDC, University of Stuttgart.

This research [44] is motivated by the global demand for building floor space, which is extensive, not only in developing countries but also in regions such as North America and Europe [45]. Current construction practices are leading to an all-time high in CO_2 emissions [45]. For instance, New Zealand faces some of the least affordable housing in the developed world, where the average cost of a home is 6–8 times the median annual household income [46], which disproportionally affects Māori and Pacifica communities, as well as younger generations [47]. Additionally, homeownership rates have declined [46,48], with many low-income families residing in older, inadequate housing stock that may negatively impact both physical and mental health [49]. Compounding the issue, New Zealand has some of the most restrictive rental conditions globally from the perspective of renters [46], while rents continue to rise [48] and in some regions outpacing income growth [49]. In response to these challenges, CFW has been proposed as a digitized and automated fabrication technology to enhance productivity in the construction industry while enabling more efficient designs and material use [44]. In this context, the substitution of carbon fibers with European flax (*Linum usitatissimum*)

fibers has been explored, leading to the first successful realization of natural fiber CFW technology demonstrators, see Fig. 1 top, proving this approach's procedural feasibility for architectural structures. As the next generation, fiber composite structures with timber elements offer a synergistic load-bearing strategy [50], see Fig. 1 bottom. In addition, fiber-based joints [51] and automated robotic assembly [52] for timber elements have also been investigated as potential peripheral advancements to CFW.

Moreover, a previous study [36] investigated the integration of various alternative fiber materials into CFW, evaluating their mechanical properties through four-point bending tests and accessing their GWP and embodied energy. The findings demonstrated that *L. usitatissimum* fibers significantly reduced GWP and embodied energy compared to carbon fibers at the same mechanical performance. This comparison also accounted for the increased quantity of fibers and resin required for weaker fiber materials. Despite the clarity of the findings, the study's broader relevance is limited, as four-point bending tests do not fully replicate the complex structural behavior of coreless filament-wound lattice components. Therefore, this paper extends the prior research by exploring a medium-scale structural system while comparing different flax fibers to a carbon fiber benchmark. Fibers made from *Phormium* (New Zealand flax), specifically *P. tenax*, are used as a primary reinforcing material in this study due to its promising mechanical properties and local availability. There is ongoing research interest in *P. tenax* fibers as a material for structural composites, involving both thermosetting and thermoplastic matrix systems [53–56]. *P. tenax* fibers exhibit several intrinsic material parameters that suggest mechanical advantages over *L. usitatissimum*, such as similar fiber strength at larger fiber diameters [55,57], higher lignin [53] as well as hemicellulose [58] contents, and less defects [59] on fiber level. Additionally, it can be sourced locally in New Zealand and other Oceanic countries, providing environmental and economic benefits. *Phormium* also carries cultural significance for the Māori people [60], further supporting its potential as a favorable material for architectural applications.

The aim of this paper is to investigate *Phormium tenax* fibers as a sustainable material option for coreless filament-wound lightweight structures. To implement *P. tenax* fibers into the CFW process, custom winding equipment, including a specially designed impregnation winding head, is developed and integrated into a robotic setup. A novel structural component design is then proposed, and samples made from *P. tenax* fibers are manufactured and mechanically tested, with carbon and *L. usitatissimum* fibers serving as benchmarks. Finally, the eco-mechanical performance of all materials is assessed.

2. New Zealand flax

New Zealand flax (*Phormium*) is a herbaceous perennial plant [61], see Fig. 2 top, endemic to New Zealand and Norfolk Island [53]. It occurs in parts of Australia, Europe, USA, and certain Pacific islands, where in some areas, it is classified as an invasive plant [61]. Assigned to the Agave family but with some distinctions [61], the plant forms a tall clump of droopy, long, green, tapering leaves with a flowering stalk extending above the clump up to five meters tall [61]. The stiff leaves can reach lengths of up to three meters and widths of up to 12.5 cm [53].

There are two species: *Phormium tenax* (Harakeke in Māori, or swamp flax) and *Phormium cookianum* (Whaririki, or mountain flax). *P. tenax* features red flowers, whereas *P. cookianum* has yellow flowers [62]. *Phormium* can be found on lowland swamps (*P. tenax*) or mountain slopes and coastal cliffs (*P. cookianum*) [62]. The leaves of *P. tenax* show the typical structure found with monocotyledons [61]. Overlapping spiral-arranged sclerenchyma fibers forming bundles parallel to the keel of the leaf; these fibers consist of elongated hollow 3–60 mm long cells with typical diameters of 5–20 μm [61]. As *P. tenax* has stiffer leaves [62] and is the common species [63], it was selected for this study. Various cultivars of *Phormium* exhibit distinct beneficial properties, making them more suitable for specific applications [64].

Fig. 2. *Phormium*. Plant (top) and fibers (bottom, extracted from another plant). Light tow (left) and heavy tow (right) yarn.

Harakeke holds profound cultural significance for the Māori people, having been traditionally used for textiles, medicine, and sailmaking [65]. During the late 19th century, harakeke was processed industrially and became one of New Zealand's most crucial export commodities [65,66]. By the early 1920s, harakeke-derived goods accounted for approximately 20% of New Zealand's total exports; however, their use declined with the rise of synthetic and sisal (*Agave sisalana*) fibers, relegating harakeke to craft applications [67]. The harakeke fiber yield can be quantified at 2.5 t/ha/a [68], compared to 2.6–4.5 t/ha/a for sisal [69]. Currently, commercial production of harakeke fibers experiences a revival [70,71].

Fibers from *Phormium* are extracted from the leaves rather than the bast, unlike with *Linum*. Despite both are being labeled "flax", they are biologically distinct as *Phormium* is a monocot while *Linum* is a eudicot. So, material properties of extracted fibers from both plants cannot be easily derived from each other. Table 1 presents the chemical composition and microfibrillar angles of several reinforcement fibers. However, the comparison of hemp (*Cannabis*), flax (*Linum*), New Zealand flax (*Phormium*), and sisal (*Agave sisalana*) reveals that hemp and flax are more similar to each other, whereas *Phormium* and sisal share greater similarities. Hemp and flax have a higher cellulose content and slightly higher moisture levels, while *Phormium* and sisal contain more hemicellulose and lignin. Extracted fibers from *Phormium* consist of multiple

Table 1
Overview of several reinforcement fibers. Chemical composition and microfibrillar angles collected and averaged from the literature [37,58,72,76–91].

Fiber	Cellulose	Hemicellulose	Lignin	Moisture	Extractives	μ-fib.angl.
Jute	57.2 ± 6.3 – 69.3 ± 2.9	12.9 ± 0.9 – 18.8 ± 2.4	9.9 ± 3.0 – 13.2 ± 1.3	10.2 – 13.7	0.5 – 1.8	7.7 – 8.6
Hemp	68.2 ± 1.1 – 76.2 ± 3.2	15.3 ± 0.6 – 21.6 ± 1.4	3.9 ± 1.0 – 7.9 ± 2.5	6.2 – 11.5	0.5 – 0.8	4.1 – 6.2
Linum	63.8 ± 1.3 – 73.7 ± 3.3	12.4 ± 4.3 – 17.6 ± 2.4	1.8 ± 0.9 – 3.6 ± 1.9	9.5 – 12.0	1.8 – 6.1	5.0 – 10.0
Phormium	48.9 ± 5.9 – 60.2 ± 8.0	23.2 ± 8.4 – 30.7 ± 6.1	6.8 ± 1.5 – 10.9 ± 2.8	7.1 – 8.9	3.7 – 4.3	18.8 – 32.0
Sisal	57.6 ± 14.1 – 69.4 ± 10.0	11.3 ± 1.0 – 29.3 ± 12.6	7.5 ± 1.9 – 10.9 ± 4.3	8.9 – 9.8	2.0 – 2.3	12.0 – 22.5
Ramie	69.9 ± 5.9 – 85.4 ± 7.0	5.5 ± 6.6 – 12.7 ± 3.6	0.5 ± 0.1 – 0.7 ± 0.1	9.2 – 16.0	0.3 – 7.7	38.3 – 47.5
Bamboo	32.7 ± 6.8 – 48.2 ± 7.8	34.0 ± 23.5 – 60.9 ± 24.2	23.1 ± 2.5 – 29.6 ± 2.4	8.8 – 10.7	2.3 – 7.4	6.1 – 8.5
	wt%	wt%	wt%	wt%	wt%	degree

hollow sclerenchyma cells limited to the length of their leave [53]. Chemical composition and, thus, mechanical properties vary based on the position along the leaves [72]. Individual *Phormium* fibers are characterized [73] as follows: a polygonal cross-sectional shape with 5 to 25 μm in diameter and relatively thick cell walls; fibers occasionally exhibiting twisting, direction being counterclockwise; along the fiber the surface is smooth with pits visible depending on the specific cultivar; the fiber ends are tapered and typically twisted. Usable fiber products are formed by overlapping of fiber hanks into bundles usually with the help of twisting, wrapping, or crocheting. *Phormium* fibers have already been used in composites with both thermosetting [74] and thermoplastic [75] matrix systems.

Fibers processed from *Phormium* leaves are called whītau in Māori [92]. In contrast to industrial extraction, fibers extracted through the traditional Māori technique [93] are more specifically referred to as muka. Different cultivars [94] vary in their suitability for fiber extraction, processing, fiber properties, and later applications [92,95]. Muka is an essential material for traditional Māori textiles, which are often woven. Māori people adhere to specific protocols [96] when harvesting leaves, which vary by iwi (tribe) and reflect traditional Māori knowledge. These protocols commonly involve (mental) preparation through prayer, following restrictions (not harvesting at night or in rain), and employing a specific cutting technique: leaves are cut diagonally from top to bottom and away from the plant's central growing point, to facilitate rainwater drainage and prevent plant die-off. Traditionally, the innermost leaf was not harvested, but the fourth leaf was favored [66]. After the leaves are harvested and trimmed, a partial transverse cut is made in the middle, allowing the muka to be separated from the leaf's flesh using a mussel shell [66]. Preferably, the leaves should be fresh at this stage. Muka is obtained exclusively from the outer (shiny) surfaces of the leaf cross-section [66,97], which generally yields the highest-quality fibers. Once both halves of the leaf are scraped, the extracted fiber hanks are usually further processed by rolling, soaking, beating, and hand-rubbing as preparation for weaving [93].

3. Material system

The samples' material system [98] consists of fiber-reinforced plastic, using either carbon or various flax fibers combined with an epoxy resin. No additional materials are included in the samples, as the winding fixture and pins are removed after curing. Carbon and *L. usitatissimum* fibers serve as benchmarks against the *P. tenax* fibers. The winding fixture used during fabrication is made of ABS (acrylonitrile butadiene styrene), while the winding pins are stainless steel. A previous study [36] indicated that analyzing embodied energy and CO_2 emissions yields similar outcomes for CFW, so this study focuses solely on GWP due to data availability and political importance. Where no product-specific data were obtainable, ranges of values from the literature had to be utilized.

3.1. Carbon fiber

A standard modulus carbon fiber roving based on PAN (polyacrylonitrile) with 48 K was selected [99] due to its balance between cost and mechanical performance, particularly its stiffness. Despite its superior mechanical properties, carbon fibers have a significantly higher mass-specific CO_2 footprint compared to natural fibers; in this study, a GWP for carbon fiber in the range of 12.55 to 31 g CO_2-eq./g was used [36]. The specific supplier was chosen based on the successful use of its products in numerous previous CFW studies. The heavier 48K product was selected to minimize the layers needed to match the higher material quantities associated with the heavy *P. tenax* fibers.

3.2. Phormium tenax fiber

In this study, two variants of *Phormium tenax* fibers were investigated, see Fig. 2 bottom, a heavier yarn with a linear density of 10840 tex and a lighter yarn with 4300 tex. Both variants were produced from leaves harvested from wild *P. tenax* plants in Riverton, New Zealand. Fiber hanks were machine-extracted from the entire leaves, which may result in lower mechanical performance compared to traditionally extracted muka fibers [74]. After extraction, the fibers were washed in water and subjected to sun and rain exposure (paddocking), which loosened non-fibrous substances that were later removed by scutching. The heavier *P. tenax* fibers exhibit a more pronounced hairiness compared to the lighter variant. To improve bundle cohesion, the *P. tenax* fiber bundles were wrapped with a polyester yarn to create a twist-less yarn (0 tpm). Cross-sectional measurements of both fiber variants were taken using two perpendicular calipers to assist in computational planning. The dry cross-sectional area of the heavier fibers is 10.28 mm^2, while the lighter fibers measure 4.92 mm^2. The lighter fibers exhibit significantly stronger intrinsic twist behavior caused by tension of the polyester wrapper. Both fiber types were rewound onto cross-wound spools before processing.

Previous studies [100] have demonstrated that alkaline treatments (> 5 wt% NaOH) on *P. tenax* fibers enhance fiber separation, which can potentially improve fiber–matrix interfacial bonding. However, such treatments also result in a reduction in tensile strength and Young's modulus [100]. Milder treatments with less concentrated alkaline solutions, on the other hand, did not significantly alter the flexural modulus or strength, suggesting that the alkaline process may remove lignin and hemicellulose, which in turn reduces the mechanical performance of the *P. tenax* fiber composite [101]. Therefore, no such treatments were applied to the fibers prior to processing in this study. Other chemical modifications to the fiber surface, such as the use of inorganic (silane) or organic (fatty acid) coupling agents, have been shown to improve wetting [102,103]. However, these methods are beyond the scope of this study.

Since there is currently no established *Phormium* fiber production industry [97], obtaining accurate sustainability parameters for the material is challenging. However, in this study, sisal (*Agave sisalana*) fibers are utilized as a proxy for the *P. tenax* fibers, given the similarities in their chemical composition, see Table 1, and fiber extraction processes: Both plants belong to the agave family, and their fibers are extracted from the leaves. Furthermore, *A. sisalana* fibers are industrially produced, for example, in South America (Brazil, Venezuela), Africa (Tanzania, Kenya, Madagascar), and Mexico, its place of origin [104]. Based on the literature, *A. sisalana* fibers have a density of 1.45 g/cm^3 [105] and a GWP ranging from 0.17 to 0.66 g CO_2-eq./g [106].

3.3. Linum usitatissimum fiber

European flax (*Linum usitatissimum*) [57] fibers have already been successfully implemented in CFW and was identified as a strong candidate for balancing mechanical performance and sustainability among various fiber materials [36]. Compared to other natural fibers, flax is particularly interesting due to its high stiffness [107]. The specific flax fibers used in this study were harvested in Upper Normandy, France [108]. Compared to both *P. tenax* variants, the *L. usitatissimum* fibers exhibit medium hairiness, a significantly less dominant twisting behavior, and a lower linear density at 1000 tex per yarn. The flax yarn is wrapped with a PET (polyethylene terephthalate) yarn to improve bundle cohesion. This fiber material has a density of 1.5 g/cm^3 [108] and the dry fiber bundle cross-section was measured as 0.505 mm^2. Based on literature [36], the GWP for *L. usitatissimum* fibers are estimated to range from 0.4375 to 0.9 g CO_2-eq./g.

3.4. Epoxy resin

Due to its excellent processing characteristics, a low-viscosity, two-component amine-activated epoxy resin was selected for sample fabrication. The specific resin product [109] was chosen for its commercial availability and similarity to resins widely used in previous CFW studies and applications. Due to supply limitations, a petroleum-based resin had to be used instead of a bio-based alternative. For the sustainability assessment in this study, the epoxy resin's GWP was estimated to range between 5.9 and 6.75 g CO_2-eq./g, noting that bio-based epoxy resins may have a potentially lower GWP.

4. Sample design

In a previous study [36], four-point bending tests were conducted to evaluate the mechanical performance of various fiber and epoxy matrix materials in CFW. The samples produced for these tests were rectangular, measuring an average of 6.6×16.4×244.9 mm^3, with unidirectional fiber placement. The samples were compressed using a metallic mold after winding to ensure parallel top and bottom surfaces. Consequently, these samples lack the geometric characteristics typical of CFW structures. Nonetheless, this method was chosen due to its simple sample geometry and well-defined loading conditions, resulting in a controlled stress distribution that allowed for an analytical comparison.

This study, however, transitions away from the previously utilized simplified sample geometry by incorporating structural characteristics unique to CFW, leading to the introduction of a novel generic sample design. Whereas load parameters for structural components can be derived from their application, determining component shape through topology optimization [110], the design options for generic samples are more numerous, as loading conditions can be arbitrarily set to match the sample's scientific purpose. In recent years, various types of generic structural samples have been established within the field [111]: Besides the four-point bending samples, the geometrically simplest are loop samples [112]. Star-shaped samples, successfully employed in various research settings [113–115], offer more complexity but demand significantly more effort regarding framing, testing adapters, and material consumption. Originally designed to investigate load induction configurations, the star-shaped samples' design favors rigidity. Inspired by the same building system, smaller cylindrical samples [36,114] offer higher syntax customization possibilities at substantially lower material consumption. However, these samples also require expensive frames and adapters. Lattice truss [25,116,117] and shell [30–32] samples simplify framing and testing requirements and allow medium-sized material consumption but lack the three-dimensional structural interactions required for this study.

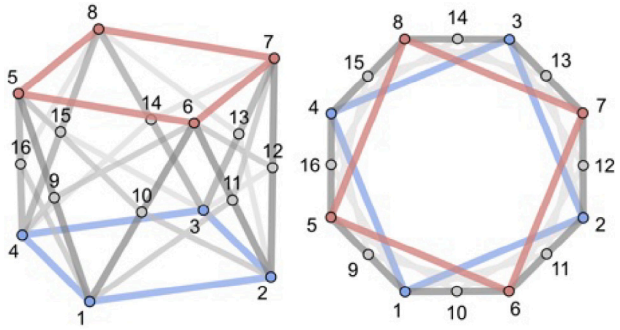

Fig. 3. Sample design. Isometric view (left) and top projection (right). Coloring for visual differentiation only. Nominal edge length (e.g. nodes 1–2) is 110 mm.

4.1. Sample topology

The novel generic sample designed in this study aims to incorporate structural characteristics of CFW while keeping the geometry as simple as possible. Essential features include fiber–fiber interactions at crossing points, layering across different sub-syntaxes, and customized rigidity throughout the loading process. The design also supports a broader range of fiber bundle diameters and reduces the need for complex framing and testing adapters. The flexibility in layering allows for fine-tuning failure modes, balancing between buckling, delamination, and fiber fracture while preventing failure near load induction regions.

The sample design, see Fig. 3, is derived from a cube with its top or bottom face rotated by 45°. Opposite corner points are connected, forming a triangular configuration of the outer predominantly load-transmitting bundles. This arrangement doubles the number of outer edges compared to a cube. Since these edges are prone to buckling under axial compression, a lateral cross-bracing was introduced to support the outer edges at their midpoint. The material distribution between these two regions can be freely adjusted through layering. When load is applied at the corners of the top faces, the upper sides of the structure buckle inward, while load applied at the top midpoints causes them to buckle outward.

4.2. Winding syntax

The embodiment of this study's design is governed by several parameters, such as dry yarn cross-section, expected fiber volume ratio, available fiber and resin quantities, workspace limitations (universal testing machine), and availability of winding fixtures. For each yarn, the cross-sectional areas of the fiber net edges are defined by the syntax. This cross-sectional area is constrained at the lower end by the structure's increasing tendency to buckle. At the upper end, it is limited by factors such as available material amounts, winding speeds, and the maximum load capacity of the testing machine. As a result, the nominal edge length of the sample was set to 110 mm, with all other geometric parameters derived from this. Next, the design space of the syntax was explored, and a variety of suitable sub-syntaxes were identified, see Table 2. These sub-syntaxes were stacked to form the final syntax based on human experience, opting for the highest possible number of layers to encourage a pronounced fiber–fiber interaction and a phased failure progression. The syntax was set as

1. single-alternating zick/zack,
2. single-alternating bracing,
3. single-alternating zick/zack,
4. non-alternating bracing, and
5. single-alternating zick/zack.

An additional reinforcement syntax for the top and bottom edges was deemed unnecessary, as alternating layering between the edge and central regions provided sufficient material coverage at the load

Table 2
Selected sub-syntaxes and layering for the sample design.

single-alternating zick/zack	$n \times$ [1, 6, 7, 3, 4, 5, 6, 2, 3, 8, 5, 1, 2, 7, 8, 4, 1]
single-alternating bracing	$n \times$ [1, 11, 7, 8, 16, 1, 2, 13, 8, 5, 10, 2, 3, 15, 5, 6, 12, 3, 4, 9, 6, 7, 14, 4, 1]
non-alternating bracing	$n \times$ [1, 11, 7, 14, 4, 9, 6, 12, 3, 15, 5, 10, 2, 13, 8, 16, 1]

With $n = 6$ for carbon, $n = 1$ for heavy tow *P. tenax*, $n = 2$ for light tow *P. tenax*, and $n = 12$ for *L. usitatissimum* fibers.

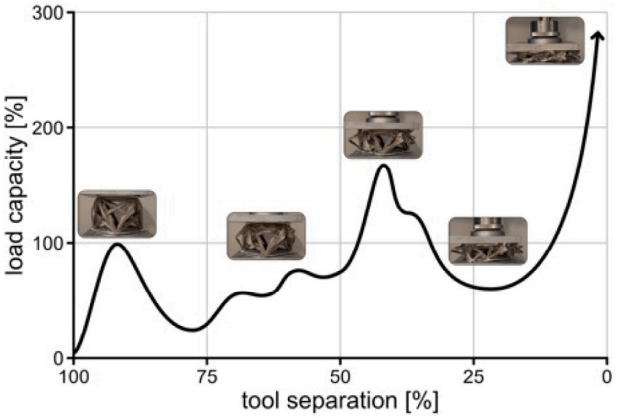

Fig. 4. Characteristic post-failure behavior for sample design. Idealized graph synthesized from mechanical testing of several samples at a higher testing speed of 20 mm/min. Tool separation at start equals sample height.

induction points. While factoring in an estimated fiber volume ratio (FVR), the material quantity was selected to maintain similar bundle cross-sections across all materials, promoting consistent failure mechanisms. This resulted in the following numbers of layers n for the different materials: six for carbon fibers, one for heavy tow *P. tenax* fibers, two for light tow *P. tenax* fibers, and twelve (3 layers with 4 yarns each) for *L. usitatissimum* fibers. To prevent lighter yarns from gaining an advantage through alternating layering, each sub-syntax is repeated individually rather than repeating the entire syntax. For maximal consistency between predicted and real-world fiber lengths, the digital model was calibrated by scaling the sample's nominal edge length to match the measured total winding length of the syntax using the actual fiber materials.

4.3. Post-failure behavior

The post-failure behavior of the sample was tested several times and represented in an idealized diagram, see Fig. 4, illustrating the varying rigidity as activation of different fiber net regions changes progresses. Initially, the outer edges fracture after buckling, causing the first peak in the diagram at 100% load capacity. As the test progresses, the core region becomes activated, leading to the second peak with its shorter buckling length. This inner core's reinforcing effect already contributes to the structure's stiffness even before the initial failure. The characteristic shape of the post-failure curve is consistent across different samples, with varying ratios between the first and second peaks for different materials.

5. Fabrication

A novel winding fixture design was developed and implemented in accordance with the novel sample design. In addition, a custom winding head was designed and implemented to accommodate the range of fiber materials used in this study, including both technical and natural fibers. The winding head features an inline impregnation system, utilizing a state-of-the-art cartridge impregnation approach [36,118]. While the winding head can be mounted on an industrial robot, sample fabrication was performed manually [112] due to the small batch size, which made automation impractical. Winding tension was actively controlled during winding. Tension fluctuations affecting pre-tensioning show no correlation with structural performance unless they alter fiber segment geometries [30]. Fiber misplacements from potential inadequate tension control would have been immediately identifiable by winding pattern deviations and remains easily correctable. Using hybrid CFW with lateral winding pins provided exceptional fiber guidance, effectively preventing misplacements.

5.1. Winding fixture

To simplify clamping and accommodate a multi-axial fiber anchoring at the samples' corners, winding pins were not deployed in the conventional way. Instead, the fibers were deposited directly onto the fixture, with lateral support provided by the pins (H=0, see Figure 7 in [12]). The fixture, see Fig. 5, also needs to be removable after the winding process, so it was designed as a modular system consisting of four identical top/bottom panels and eight identical side panels. These panels were produced using ABS material via a fused deposition modeling 3D-printer, printed at low resolution with minimal infill to reduce production time. The printed fixture enables cost-effective panel production while ensuring a smooth fiber deposition surface at the fixture's corners in contrast to a winding fixture assembled from laser-cut plat panels. It also allows for precise angular orientation of the winding pins. To achieve sufficient rigidity during winding, the fixture was designed as a self-locking shell structure, with the four top/bottom parts acting as keystones to prevent the structure from loosening during the winding session. This procedure ensures that the fixture supports all fiber segments from the inside, making the winding process a hybrid form of coreless filament winding. The ABS fixtures were assembled by applying cyanoacrylate adhesive to the adjacent surfaces and welding the edges together using a soldering iron. This welding process also smoothed the fiber deposition areas and filled any potential gaps between panels. For the winding pins, 5 mm diameter by 35 mm long dowel pins were coated with a mold release agent and press-fitted into the fixture's holes. After the winding process and curing of the resin, the fixtures were mechanically disassembled. The top and bottom parts were removed first, allowing the side panels to be separated from the fiber composite and taken out through the top or bottom openings. Any remaining ABS material on the inside of the fiber composite structure was also mechanically removed. The use of water-soluble PVA (polyvinyl alcohol) for the fixture was not chosen, as mechanically removing the ABS panels proved more time-efficient.

5.2. Winding head

The winding head, see Fig. 6 consists of both SLS 3D-printed and laser-cut components. The impregnation chambers are secured by a 3D-printed holder, based on a previous design [36,118]. This updated version features an additional 3D-printed holder at the top of the upper cartridge, which serves multiple functions: it provides a large radius and smooth inlet to accommodate fibers approaching from various angles and includes a lateral opening for resin supply. Pre-mixed resin can be delivered through this opening, for instance, using a peristaltic pump, similar to previous designs [118]. The opposite end of the impregnation head holds a nozzle, mounted with another 3D-printed holder. The nozzle's inner diameter is set to accommodate the heavier *P. tenax* fibers but can also be used with lighter fibers. To reduce leakage, the lower opening of the impregnation cartridge can

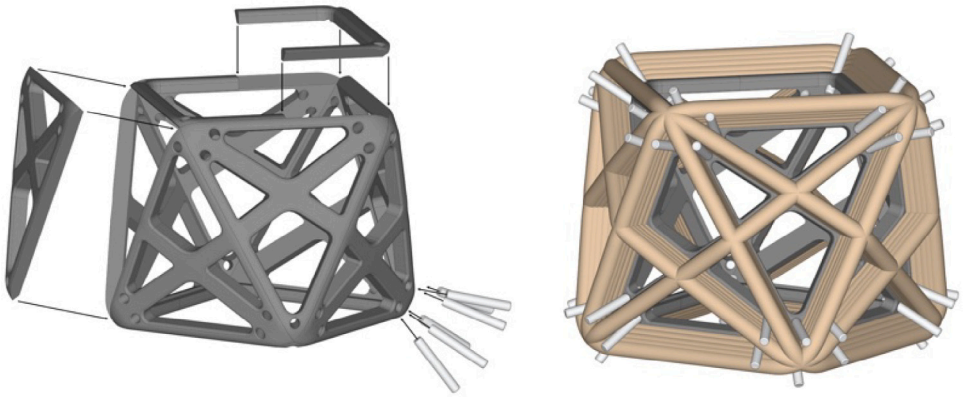

Fig. 5. Winding fixture. Left: Assembly consisting of eight identical side panels, four top/bottom pieces, and six winding pins per corner. Right: Schematic illustration of the fixture with fiber composite material applied.

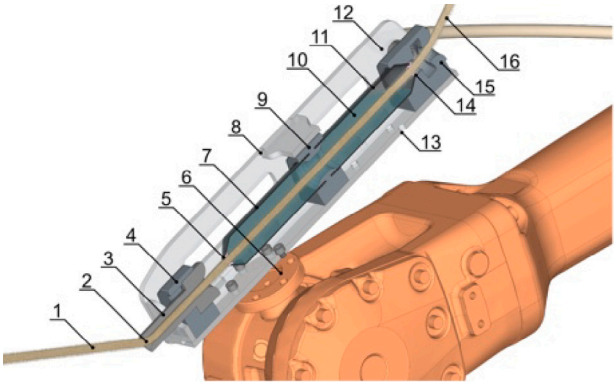

Fig. 6. Sectional view of the impregnation winding head. 1: impregnated fiber, 2: tool center point, 3: nozzle, 4: nozzle holder, 5: lower outlet eyelet, 6: lower mount to robot, 7: lower impregnation cartridge, 8: frame of the winding head, 9: cartridge holder, 10: resin reservoirs, 11: upper impregnation cartridge, 12: resin inlet, 13: upper mount to robot, 14: upper inlet eyelet, 15: resin inlet holder, 16: dry fiber arriving from fiber source.

be equipped with several eyelets designed for different fiber diameters. Characteristic nozzle diameters per yarn/roving are 2.8 mm for carbon, 7.0 mm for heavy *P. tenax*, 4.9 mm for light *P. tenax*, and 2.0 mm for *L. usitatissimum* fibers. A wider cone-shaped cavity at the inlet of the nozzle prevents resin leakage by catching excess resin. The tool center point (TCP) is positioned at the midpoint of the lower nozzle opening, and the nozzle can be passively raised to prevent damage during potential collisions. The frame of the impregnation winding head was laser-cut from PMMA (polymethyl methacrylate) and can be directly mounted to the robot flange [119] in two configurations for automated winding operations.

5.3. Fabrication process

The winding process in this study followed the state-of-the-art approach used in CFW [17,18,118], with the distinction that the winding head remained stationary while the winding fixture moved to follow the winding trajectory. Before winding, the fiber spools were dried in an oven to set the moisture content [120] of the natural fibers. The fiber source was fixed externally, and the winding head was centrally positioned above the workspace to prevent fiber damage by minimizing the angle between the nozzle and the fiber during winding. No severe differences in the processability of *P. tenax* and *L. usitatissimum* were observed — the processability of natural fibers in CFW is extensively documented in [36,121]. After winding, all samples were suspended, maintaining consistent orientation during curing and, thus, resin distribution. Once cured, excess fiber strands and winding pins were removed, and the fixture was destructively disassembled. Finally, the samples, see Fig. 7, were tempered before the mechanical tests.

5.4. Sample parameters

After drying the fiber spool and after the winding process, the weights of the spools were recorded. After demolding, the total weight of each sample was measured and samples were labeled. Based on these measurements, the fabrication-related sample parameters were calculated, see Fig. 8, using established methods [36]. The fiber mass was determined from the difference in spool weights, accounting for any potential cut-offs and neglecting potential moisture gains during winding. For cut-off fiber segments, an estimated fiber mass ratio (FMR) per fiber material was used to calculate their dry fiber weight. The resin mass was then derived from the total composite weight of the sample, and from this, the FMR was calculated. The FMR was converted to the FVR, see Eq. 1 from [36]. The diameters of the outer edge bundles can be measured using calipers and other standard methods [31]. However, in this study an alternative approach was required due to the rough surfaces of natural fibers. Fiber and resin volumes were calculated from the fiber and resin masses, using their material densities. Based on the total composite volume and the material distribution defined by the winding syntax, the volume was assigned to the different regions of the fiber net. From this, cross-sectional areas of individual segments were computed, allowing the bundles diameters to be approximated under the simplification that fiber net edges could be represented as cylindrical.

The FVR arises based on process parameters and cannot be arbitrarily adjusted by state-of-the-art winding system. The significantly higher FVR (and fiber mass) observed in carbon fibers at 57.4% can be attributed to better chemical compatibility between the fiber and resin materials compared to the natural fibers with an average of 27.6%. The heavy *P. tenax* fiber exhibited the highest variation in FVR at 2.9%, which may result from the lower cohesion between individual fibers and less efficient packing of yarns, allowing more resin to accumulate. Considering the high variations inherent to CFW, the average outer edge diameter at 9.4 mm^2 ± 8.9% remains relatively constant between samples. The total composite mass fluctuates more across samples, averaging 317 g ± 15.4%. As expected, variations in both bundle diameter and resin mass were more pronounced in natural fibers compared to carbon fibers, whereas variation in FVR are similar.

The GWP contribution of each material was calculated based on mass-specific values found in the literature. The CO_2 emissions from the winding process and tempering were excluded, as they were consistent across all samples and relatively minor compared to the GWP of the

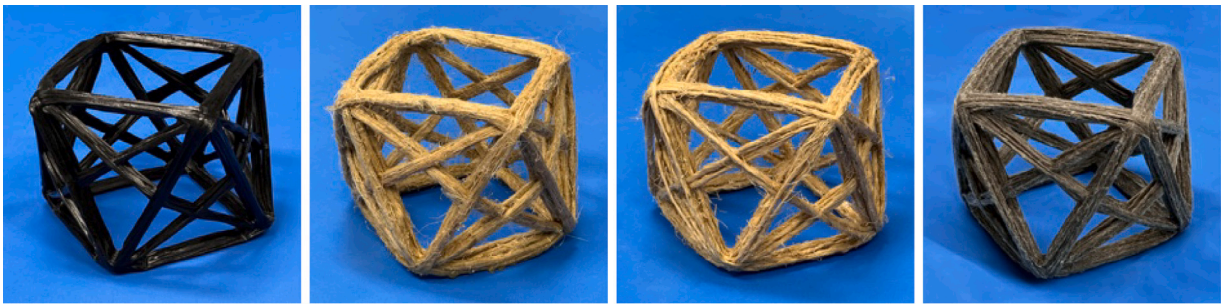

Fig. 7. Samples made from different fiber materials. Carbon fiber, heavy *P. tenax* fiber, light *P. tenax* fiber, and *L. usitatissimum* fiber (left to right).

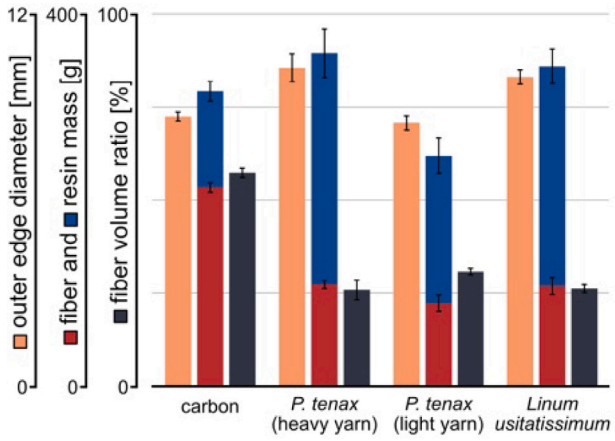

Fig. 8. Fabrication-related parameters of samples. Fiber (red) and resin (blue) mass add up to composite (red+blue) mass. The outer edges are all edges similar to edge 1–6, see Fig. 3. Outer edge diameter represent the composite volume of the sample.

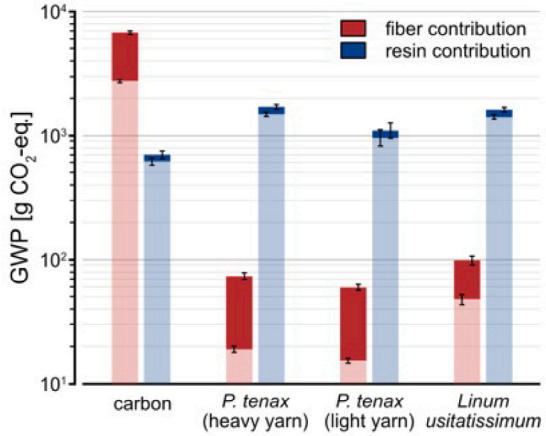

Fig. 9. Global warming potential. CO_2-eq. contribution of fiber and resin separated. Span results from the range in GWP values for material from literature. Standard deviations result from variance between samples. Ordinate in log. scale.

raw material production. The CO_2 emissions for fibers and resin were calculated separately by multiplying the fiber or resin mass in each sample by the respective mass-specific GWP value for the material, see Fig. 8 and Section 3. Due to significant variability in the reported GWP values for the same material across different studies, a range (dark-colored area) was used, see Fig. 9, whereas standard deviations were derived from the sample data (n = 5) for each material.

As expected, the GWP contribution of carbon fibers is several magnitudes higher than that of natural fibers. In fact, the contribution from natural fibers is almost negligible when compared to both carbon fiber and the resin contributions. Due to the lower FVR in natural fiber samples, the amount of resin required per sample was higher than in the carbon fiber samples, resulting in a correspondingly higher GWP contribution from the resin in natural fiber samples. The light *P. tenax* fiber exhibit the lowest resin contribution among the natural fibers, but also the highest standard deviations. Overlapping standard deviation bars in Fig. 9 indicate that the variability within the fabrication process is greater than the variation due to the range of literature GWP values.

When considering the absolute fiber and resin contributions to GWP, the natural fiber samples show a substantial improvement, requiring on average only 26.5% of the GWP of the carbon fiber samples. The light *P. tenax* fiber exhibited the lowest GWP, at 19.7%, while *L. usitatissimum* and heavy *P. tenax* fibers were similar, both contributing around 29.9% of the GWP of the carbon fiber sample. The larger variability in reported GWP values for natural fibers, particularly for *P. tenax* fiber, led to a wider spread in their fiber GWP contributions, see Fig. 9. This analysis, however, does not account for mechanical performance parameters.

6. Structural analysis

6.1. Testing setup

Using a 100 kN spindle-driven universal testing machine, the samples were subjected to a displacement-controlled quasi-static compression structural test, see Fig. 10. Contrary to conventional testing methods, the samples in this study were not bolted to the machine's adapter due to the absence of winding anchors. Instead, the samples were placed between two metal plates with a consistent orientation (winding point 1 at the bottom rear). Silicone rubber sponge sheets (1.5 mm thick, 1.25 g/cm^3, 60 ± 7 Shore A) [122] were placed above and below the sample to equalize load induction and prevent sliding. A pre-load of 250 N was applied, which includes the weight of the upper metal plate and rubber (90 N). The load cell was mounted above the sample and the testing speed was set to 1 mm/min. For the further analysis in this study, the failure load and structural stiffness parameters of each sample, see Fig. 12, were extracted from the load–displacement curves before initial structural collapse. The failure load was identified as the maximum force, while the structural stiffness was determined by calculating the slope of the curve at intervals of every 140 μm displacement and selecting the maximum value. Accurate determination of the structurally relevant cross-sectional area throughout testing was not possible; therefore, conversion into compressive strength or modulus are not feasible.

6.2. Failure behavior

The failure behavior of all samples followed a consistent pattern, see Fig. 11. Initially, there was an onset of deformation attributed to clamping, which transitioned smoothly into a linear-elastic regime. In contrast to other CFW structures, no reconfiguration of the composite material was observed during the Hookean regime, typically

Fig. 10. Compression testing setup.

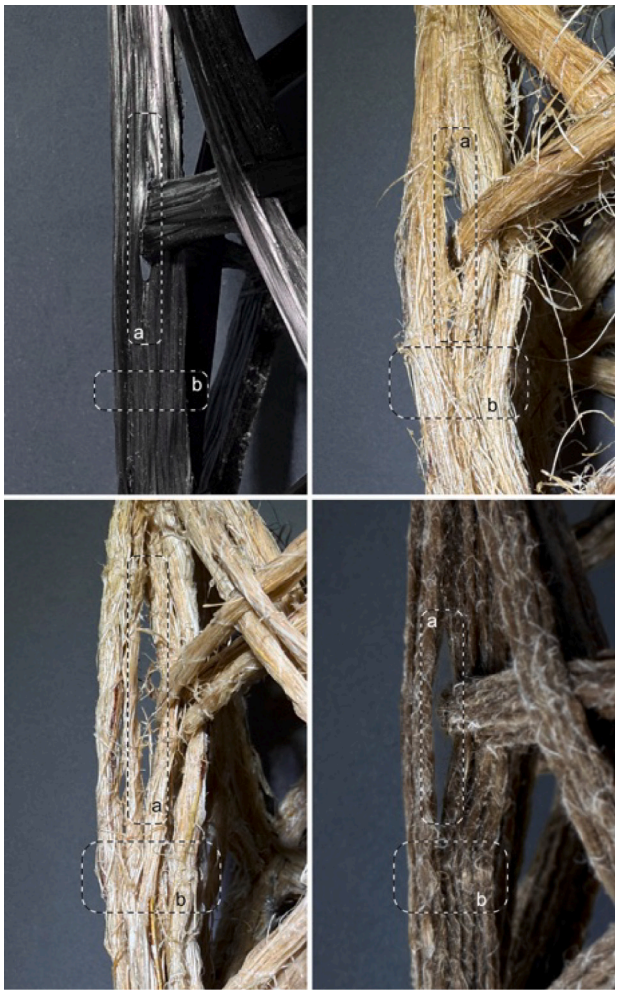

Fig. 11. Failure patterns observed during compression testing. Carbon, heavy and light yarn *P. tenax*, and *L. usitatissimum* fiber (top left to bottom right). Regions of delamination (a) and fiber fracture (b) marked. The fiber fracture in the carbon fiber sample is barely visible, as these samples show almost no global plastic deformation after unloading due to their rebound behavior.

introduced by winding anchors, which were absent in this sample design. As the loading continued, a gradual reduction in structural stiffness was evident, accompanied by outward buckling of the outer edges. At a certain point during this decline in stiffness, delamination, defined by the interlaminar fracture toughness [123] of the material system, occurred as the outer layers of the edges detached from the underlying lateral cross-bracing sub-syntax. The debonding of the outer edges increases their free length and hence their tendency to buckle, resulting in a reduced strut failure load, which is controlled by fiber fracture occurring later. This delamination, see Fig. 11a, was not clearly reflected in the force–displacement graph but indirectly influenced the failure load values of the sample. The resistance to delamination (debonding of the outer edges) depends on material properties (fiber–matrix adhesion, matrix strength) and processing parameters (FVR and winding tension, affecting contact area). However, determining the delamination resistance is beyond the scope of this study. With the progression of global buckling, the structural stiffness decreased further until a fiber fracture occurred in the buckled outer bundles, see Fig. 11b, resulting in a significant drop in load after the failure load was reached, marking the end of the test, see 100% load capacity in Fig. 4.

6.3. Mechanical performance

The carbon fiber samples exhibited significantly higher mechanical performance, bearing 4.3× the load and 6.0× the stiffness of average natural fiber samples, see Fig. 12. Among the natural fibers, *L. usitatissimum* outperformed both *P. tenax* in terms of stiffness and failure load at a factor of 1.8× and 1.4×, respectively. *L. usitatissimum* also showed the lowest standard deviation (9% and 4%) in both parameters, due to the fact that its yarn is more optimized for composite processing. Additionally, the thinner yarn of *L. usitatissimum* facilitates more homogeneous packing across the entire cross-section. In terms of variability, the heavy *P. tenax* fiber showed the largest standard deviation in stiffness (35%), while the light *P. tenax* fiber exhibited the greatest fluctuation in load capacity (30%). The carbon fiber samples exhibit an average standard deviation of 15% for both mechanical performance indicators, aligning with the expected range for structural testing of CFW components with this yarn-to-component size ratio. Among the evaluated samples, carbon fiber exhibits the highest stiffness-to-load-capacity ratio at 18%, followed by *L. usitatissimum* at 15%; in contrast, both *P. tenax* fibers demonstrate significantly lower values, around 11%, highlighting the importance of *L. usitatissimum* fibers in structural designs prioritizing high stiffness. From a structural point of view, the heavy *P. tenax* fiber is superior to the light *P. tenax* fiber as it provides 2.1× the structural stiffness and 1.9× the load capacity.

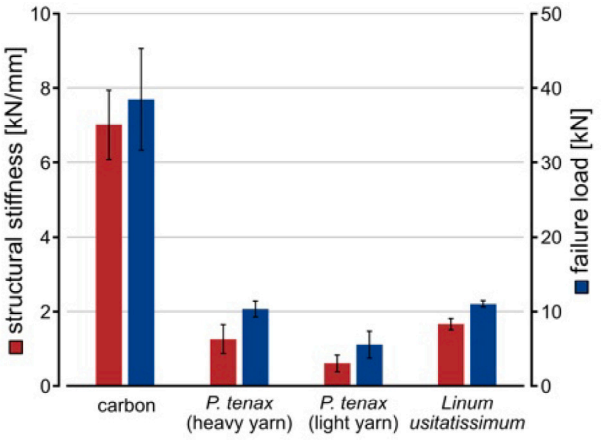

Fig. 12. Structural stiffness and failure load results from quasi-static compression testing. Absolute values. Failure load equals 100% load capacity, compare Fig. 4.

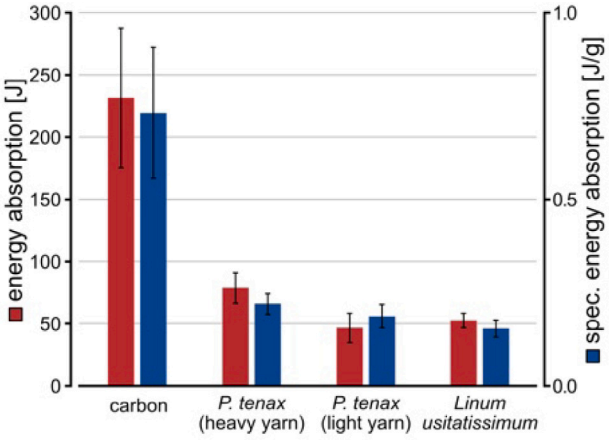

Fig. 13. Energy absorption of samples up to the failure load. Specific energy absorption calculated based on composite mass, see Fig. 8.

6.4. Energy absorption

Furthermore, the absolute energy absorption (EA) and composite mass-specific energy absorption (SEA) of each sample were calculated from the quasi-static structural compression testing load–displacement curves by integrating from the start of the test until the displacement at which the failure load was reached, using the composite trapezoidal rule, see Fig. 13.

The carbon fiber samples exhibited the highest energy absorption, with both EA and SEA values reaching 3.9× those of the natural fiber samples. Among the natural fibers, EA and SEA values are more similar to each other compared to the differences observed in the mechanical performance data, see Fig. 12. However, a different trend was observed: *P. tenax* heavy yarn showed the highest energy absorption, with EA and SEA values reaching 1.5× and 1.4× those of *L. usitatissimum*, respectively. The *P. tenax* light yarn exhibited an average energy absorption similar to that of *L. usitatissimum*, with EA values at 1.2× and SEA values at 0.9× that of *L. usitatissimum*. Notably, the *P. tenax* light yarn stood out for its relatively higher SEA compared to its own EA. The observed differences in energy absorption may be attributed to the material parameters of the dry fibers, but they are more likely a consequence of the layering effect in the CFW composite structure. Carbon fiber exhibited the highest relative standard deviations among all tested materials, with an average of 24% for both EA and SEA, whereas *L. usitatissimum* reaches 12%. The larger variations observed in carbon fiber are artifacts of the testing plan and are expected to disappear with larger sample sizes.

P. tenax exhibits greater toughness than *L. usitatissimum*. However, energy absorption will not be further discussed in this study, as the structural design in intended applications is not driven by dynamic, cyclic, or impact load conditions.

7. Sustainability evaluation

After defining the eco-mechanical indicators, following a similar approach to that used by Cáceres et al. [124] on tailored fiber placement, both indicators were applied to the samples as produced (similar cross-sectional area) and in a second analysis step to a scenario with samples at equal fiber mass (reduction based on scalability for CFW carbon sample). Finally, an estimation is provided for improved FVRs, based on the assumption that mass-specific mechanical performance remains constant while only the resin mass adjusts.

7.1. Eco-mechanical performance indicators

To assess the overall performance of the samples, including lightweight potential and the sustainability of the materials used, two performance indicators were defined as

$$k_{\text{spec}} = k/(m_c \text{ GWP}) \quad (1)$$

$$F_{\text{spec}} = F/(m_c \text{ GWP}) \quad (2)$$

with

k_{spec} spec. structural stiffness [N/(g^{2}m)];
F_{spec} spec. failure load [N/g^2];
k structural stiffness [N/m], see Fig. 12;
F failure load [N], see Fig. 12;
m_c composite mass [g] of sample, see Fig. 8; and
GWP global warming potential [g CO_2-eq.] of entire sample, see Fig. 9.

This approach was selected as an preferred analytical or numerical mechanical comparison was not feasible due to the uncontrolled meso-scale sample geometry, unknown load induction distribution, and transient stress distribution along the fiber net. Both eco-mechanical performance indicators normalize structural stiffness or failure load specific to composite mass and GWP of the sample. They are calculated separately and averaged afterward to preserve information about deviations between samples. The GWP range for the individual materials are represented as low-high values. Absolute mechanical performance or processability are not included and need to be evaluated separately. With the indicators defined as they are, the balance between lightweight performance (mass-specificity) and sustainability performance (GWP-specificity) is maintained, meaning that in the further analysis, 1 g of composite mass is equally weighted to 1 g of CO_2 equivalent.

7.2. Comparison at similar cross-sectional area

The first analysis, see Fig. 14, was conducted on the samples as they were fabricated, with similar bundle cross-section, see parameters from Fig. 8. The standard deviation reflects the variation between different samples within each batch, while the range (blue and red boxes) represents the GWP range reported in the literature for the materials used, see Fig. 14.

Carbon fiber samples exhibit the best eco-mechanical performance among the investigated materials, particularly in terms of specific stiffness. The range for the carbon fiber sample's indicators are also the largest because of the variability in GWP values. Natural fiber samples

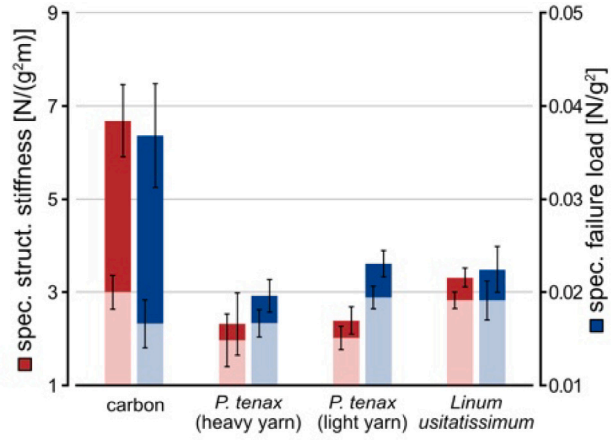

Fig. 14. Eco-mechanical performance. Specific stiffness k_{spec} and specific failure load F_{spec} for samples as fabricated (similar bundle cross-sectional area). Standard deviations result from variance between samples.

perform at a similar level and on average reach 59% of carbon fiber samples in terms of specific stiffness and 87% for specific failure load. Among natural fibers, *L. usitatissimum* generally outperforms *P. tenax* fibers, with the exception of light *P. tenax* fibers, which demonstrates marginal higher specific failure load. Both *P. tenax* fiber types, on average, achieve 70% of the specific stiffness of *L. usitatissimum*, with heavy *P. tenax* fibers reaching 87% of its specific stiffness. Previous research [74] suggests that hand-decorticated flax fibers exhibit significantly higher mean tensile strengths compared to those extracted by machine. This might be advantageous for the *P. tenax* fibers where hand decortication continues to be practiced due to its cultural importance. The most pronounced variation between samples is observed in heavy *P. tenax* fibers, while *L. usitatissimum* shows the least variation. Despite the higher mechanical performance of heavy *P. tenax* fibers, the inclusion of GWP in the overall analysis favors light *P. tenax* fibers, underscoring the significant impact of FVR. The heavy *P. tenax* fibers samples contain considerably more resin, negatively influencing its eco-mechanical performance. This first analysis implies that when cross-sectional area is the primary design criterion and FVR values remain representative, carbon fiber is the superior eco-mechanical material choice for both stiffness and failure load driven applications.

7.3. Comparison at equal fiber mass

In the second phase of analysis, the focus shifts to assessing performance based on fiber mass as the key design parameter, rather than cross-sectional area. To achieve this, the scalability of the mechanical performance relative to fiber mass was approximated first. As the fiber mass among the natural fiber samples is already similar, only the parameters for the carbon fiber samples must be adjusted to a reduced fiber mass, see Fig. 8. An additional carbon fiber sample, fabricated with half the layers (n = 3, see Table 2) of the standard sample, allowed for an interpolation of how fiber mass affects stiffness and load capacity:

$$k_{\text{int}} = 0.4396\ m_f^{1.8013} \qquad \text{with } R^2 = 89.17\% \tag{3}$$

$$F_{\text{int}} = 32.0236\ m_f^{1.3187} \qquad \text{with } R^2 = 73.96\% \tag{4}$$

with k_{int} interpolated structural stiffness [N/mm], see Fig. 12; F_{int} interpolated failure load [N], see Fig. 12; and m_f fiber mass [g] of the carbon fiber sample, see Fig. 8. This interpolation was then applied to recalculate the mechanical performance of the regular carbon fiber samples (n = 6) for a reduced fiber mass that matches with the average fiber mass of the natural fiber samples, thereby preserving the variation among the carbon fiber samples. As already shown in a previous study [116], the material scalability in CFW does not follow a linear trend. However, it should be noted that the reliability of the interpolation is constrained by the limited sample size used in this study. In comparison to the analysis based on a constant cross-sectional area, see Fig. 14, this second analysis, see interpolated structural stiffness (red) and interpolated failure load (blue) in Fig. 15, does not alter the overall trend. However, in absolute terms, the advantage of carbon fibers over natural fibers decreases slightly.

7.4. Variation of fiber volume ratio

Building on the previous analysis, the next step examines the potential effects of improved FVR for the natural fibers. Similar to the earlier approach, the mechanical performance was evaluated across varying FVRs based on the fabricated and tested samples. However, no reliable equation could be derived for extrapolation, as the relationship between mechanical performance and FVR was found to be strongly scattering across the entire range of the measurements. In addition, the FVR values of the tested samples were not sufficiently spread to yield reliable trends for extrapolation. As the FVR increases, a negative linear trend is expected until a specific FVR is reached, where the failure mode shifts from matrix- to fiber-controlled, beyond this point, a positive linear trend is anticipated [125]. Therefore, an alternative approach was used, the mass-specific mechanical performance was assumed to remain constant, while the resin mass and corresponding GWP were adjusted based on hypothetical adjustments in FVR. In Fig. 15 the eco-mechanical performance indicators for equal fiber mass are shown with original (as fabricated) FVR in red and blue, while values for the hypothetical FVRs are shown in gray. Although this projection is a simplified model, it offers a valuable outlook on how enhanced FVRs may influence the eco-mechanical performance in the future, when fabrication setups will have improved; potentially impacting material selection decisions. Previous research [126] on *P. tenax* fibers composites has shown that mechanical performance increases with FVR, but this trend is strongly altered by the applied treatments. A linear trend for modulus and an exponential trend for strength can be expected between 20%–50% FVR. [68]. Higher FVRs of over 50% have already been achieved with *P. tenax* fibers and epoxy matrix using a vacuum infusion process [74]. However, the bagging required for vacuum sealing may be too time-consuming for lattice structures, whereas integrating [18] pultrusion characteristics into the winding process could potentially facilitate increasing FVRs.

Similar to Fig. 14, the carbon fiber samples demonstrate high baseline values for both specific stiffness and specific failure load, clearly outperforming the natural fibers. For the natural fiber samples, both specific structural stiffness and failure load show significant capacity for improvement with increasing FVR. As the FVR approaches values around 45%, the performance of the natural fibers begins to approach that of the mid-range carbon fiber samples. *L. usitatissimum* demonstrates the highest improvement potential for structural stiffness with increasing FVR. Besides the inherent differences in the raw material's structural stiffness, this might suggest that the original FVR for *L. usitatissimum* may be closer to its optimal value than *P. tenax* fibers. In terms of failure load, both *P. tenax* fibers and *L. usitatissimum* exhibit similar improvements as FVR increases. The heavy *P. tenax* fibers is slightly more sensitive to changes in FVR compared to light *P. tenax* fibers for both indicators, but particularly in terms of structural stiffness. However, the heavy *P. tenax* fibers also show the highest variation between samples. All natural fibers exhibit more significant variability between samples compared to carbon fibers. It is important to note that the increasing size of the error bars with higher FVR is an artifact of the mathematical extrapolation and may not necessarily reflect reality. Similarly, the uncertainty range for GWP values also increases with higher FVR.

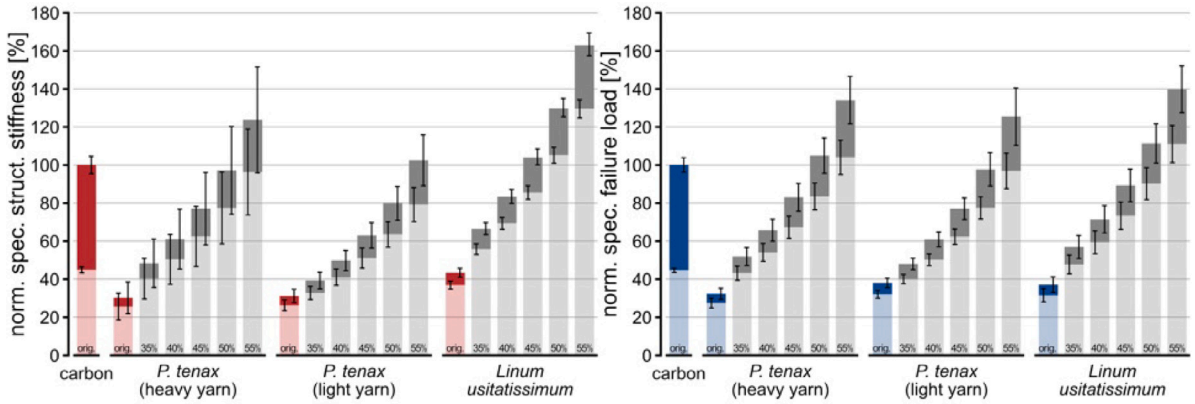

Fig. 15. Specific structural performance individually normalized to the maximum values of carbon fiber samples and with several FVR for natural fibers. Structural stiffness and failure load values for carbon fiber samples were interpolated to maintain similar fiber mass across all materials, compare Fig. 14. Average percentage FVRs as originally fabricated are 57.4 ± 2.0 for carbon, 25.8 ± 1.3 for *P. tenax* fibers heavy yarn, 30.8 ± 2.9 for *P. tenax* fibers light yarn, and 26.1 ± 1.1 for *L. usitatissimum*. Standard deviations result from variance between samples. Performance indicators for FVRs between 35%–55% were extrapolated assuming constant composite-mass-specific stiffness and failure load values for each material.

At the original FVRs, the carbon fibers clearly outperform the natural fibers. However, the projection indicates that with improved CFW fabrication techniques and raw material processing, natural fibers, particularly *L. usitatissimum* and heavy *P. tenax* fibers, may close the performance gap significantly. Among the natural fibers, *L. usitatissimum* shows the highest potential, but it is also more optimized for composite processing compared to *P. tenax* fibers. Between the two tested *P. tenax* fibers, the heavy *P. tenax* fibers appears more promising due to its higher absolute mechanical performance, see Fig. 12, and greater sensitivity to eco-mechanical improvements through increased FVR, see Fig. 15. However, the baseline eco-mechanical performance of heavy *P. tenax* fibers is lower than that of light *P. tenax* fibers, see Fig. 14, and it also exhibits significantly higher variability between samples in some parameters, see Figs. 8, 12, and 15.

8. Discussion

This study proposes *P. tenax* fibers as reinforcement material for coreless filament-wound lightweight structures. It explores their eco-mechanical performance within a novel structural system, benchmarking them to carbon fibers and *L. usitatissimum* fibers. The ultimate aim is to contribute to more sustainable practice in the AEC sector, particularly in New Zealand.

Building on previous research, this study introduced a novel sample design featuring higher structural complexity. Samples were produced from two product types of *P. tenax* (heavy and light yarn), carbon fibers, and *L. usitatissimum* fibers. To achieve this, a 3D-printed winding fixture and a custom winding head were developed and integrated into a robotic setup. The mechanical performance of the samples was evaluated through destructive compression tests. Eco-mechanical performance indicators were defined and accessed, combining the material's global warming potential and the samples' mass-specific structural performance.

While carbon fibers outperformed natural fibers at their original fiber volume ratios, the findings suggest that advancements in raw fiber processing and CFW techniques could enable natural fibers, especially *L. usitatissimum* and heavy *P. tenax*, to approach the performance of carbon fibers. *L. usitatissimum* exhibited the highest potential among natural fibers. In contrast, heavy *P. tenax* yarn demonstrated greater promise due to its superior absolute mechanical performance. However, it also exhibited larger variance in some parameters between samples and lower baseline eco-mechanical performance compared to light *P. tenax* yarn.

Aside from the main research question, the novel design proposed in this study expands the existing range of generic sample types for CFW. Key features include its ability to incorporate essential structural characteristics, flexibility in layering and sub-syntax configuration, customizable rigidity and post-failure behavior, and accommodation for various fiber bundle diameters. In addition, the design simplifies load induction and reduces the risk of failure near these regions.

The study encountered several methodological limitations. GWP values are estimates based on literature and not determined for specific materials. Due to fabrication effort and material availability, the number of samples is limited. Therefore, the significance of mathematical approximations for the performance indicators is also constrained. Non-identical equipment across different laboratories had to be utilized but with consistent procedures. As common in CFW, the results are specific to the tested structural system. Variations in the building system configuration or future advancements in CFW fabrication techniques could alter the findings substantially. In particular, improvements in fiber impregnation technology, which is expected to advance in the near future for natural fibers, could affect the relevance of the findings.

Further optimization of *P. tenax* fibers targeted toward composite processing holds enormous potential for performance enhancements, especially in comparison to the already highly optimized *L. usitatissimum* fiber products available. Besides improving yarn characteristics to enhance processability, such advancements must address fiber-resin bonding.

This study represents a significant step toward integrating *P. tenax* fibers into structural composite applications, particularly in the AEC sector. While previous research emphasized the material level and thus suggested the unchallenged superiority of natural fibers over carbon fibers in terms of eco-mechanical performance, this study extends these findings to a structural level. The results highlight that material selection cannot rely solely on individual material properties; structural behavior within a system must also be considered. The optimal choice between conventional high-CO_2-impact fibers and natural fibers depends on the designer's decision to balance sustainability and lightweight performance requirements, which may vary enormously depending on the application. Therefore, for lightweight applications (aerospace or automotive) where energy consumption during the product's lifespan outweighs energy use during material sourcing and production, carbon fibers prove to be the optimal choice for many highly-stressed components. Conversely, natural fibers can enhance sustainability when appropriately integrated, as demonstrated by other research [35] combining flax fibers and timber into a hybrid system.

9. Conclusion

Structural samples made from carbon, *Phormium tenax*, and *Linum usitatissimum* fibers with epoxy resin were destructively tested under quasi-static compression. Carbon fiber samples demonstrate mass/CO_2-specific stiffnesses and failure loads that reach 2.18× and 2.12×, respectively, the average natural fiber values. The mass/CO_2-specific stiffness among *P. tenax* yarns with different linear densities is similar and at 71% of that of *L. usitatissimum* samples. For mass/CO_2-specific failure loads, both *P. tenax* fibers exhibit similar values to *L. usitatissimum* samples, with the heavy yarn at 87% and the light yarn at 102% of the *L. usitatissimum* value. A significant increase in fiber volume ratio could help close the performance gap between carbon and natural fibers, with *L. usitatissimum* being more sensitive to changes. Furthermore, mass-specific energy absorption (SEA) was evaluated; where carbon fiber samples achieve 3.9× the SEA of average natural fiber samples. *P. tenax* samples reach SEA values at 1.3× that of *L. usitatissimum* fiber samples, with the heavy yarn showing better absorption than the light yarn. The experimental findings indicate that, at the structural level and for the investigated sample design, the natural fibers do not outperform carbon fibers in terms of eco-mechanical performance when using the current CFW fabrication technology, the available resin systems, and when balancing lightweight and sustainability importance equally.

Despite the current challenges, *P. tenax* fibers show great potential as a sustainable fiber material, particularly in New Zealand, where its cultural significance and local availability make it an attractive option for construction materials. Natural fiber composites have demonstrated successful application in load-bearing structures within research demonstrator building systems [34,35] over extended periods. However, future research could investigate the long-term durability of *P. tenax* composites through accelerated weathering tests, with specific emphasis on the matrix and the fiber–matrix interface. Typically, matrix discoloration serves as an indicator of reduced molar mass and deterioration of mechanical properties, while moisture absorption may induce material swelling, internal stress development, and degradation of the fiber–matrix interaction [120,127]. Moreover, existing design methodologies could be adapted to efficiently incorporate the elevated material consumption of natural fiber composites compared to technical fiber systems to harness the full potential of natural fibers. Furthermore, a possible future use of *P. tenax* fibers in sustainable building construction, combined with the material's cultural importance to the Māori people, could provide a chance to express Māori culture and knowledge through architectural design [128]. Traditional extraction methods of *P. tenax* fibers could yield higher mechanical properties of CFW structures, but are not scalable to an industrial level. However, the most substantial improvement in the sustainability of natural fiber composites will not stem from fiber optimization but from reducing the environmental impact of the matrix system, potentially through bio-based epoxy systems.

CRediT authorship contribution statement

Pascal Mindermann: Writing – original draft, Visualization, Supervision, Software, Project administration, Methodology, Investigation, Funding acquisition, Formal analysis, Data curation, Conceptualization. **Yifan Lv:** Investigation. **Malaya Prasad Behera:** Investigation. **Romain Meot:** Validation. **Marie-Joo Le Guen:** Writing – review & editing, Validation, Resources. **Sarat Singamneni:** Writing – review & editing, Resources, Conceptualization.

Funding

This research was partially supported by the Deutsche Forschungsgemeinschaft (DFG; German Research Foundation) under Germany's Excellence Strategy – EXC 2120/1–390831618. This work was supported by the New Zealand Ministry of Business, Innovation and Employment through the Strategic Science Investment Fund for Scion's Manufactured Products From Trees science platform (Contract number C04X1703). The experimental progress made at the Auckland University of Technology was supported by the funding from the New Zealand Product Accelerator.

Declaration of competing interest

The authors declare the following financial interests/personal relationships which may be considered as potential competing interests: Pascal Mindermann reports financial support and travel were provided by German Research Foundation. Marie-Joo Le Guen reports financial support was provided by New Zealand Ministry of Business Innovation and Employment. Sarat Singamneni reports financial support was provided by New Zealand Product Accelerator. If there are other authors, they declare that they have no known competing financial interests or personal relationships that could have appeared to influence the work reported in this paper.

Acknowledgments

Māori ownership, traditional knowledge, and the status of plants investigated in this work under Article II of The Treaty of Waitangi are acknowledged and recognized by the authors. The authors thank their fellow researcher Marie-Joo Le Guen, the Biopolymer Network Ltd, and AgResearch New Zealand for providing the *Phormium tenax* fiber yarn. The authors also like to acknowledge the discussions with Prof. Raechel Laing of Otago University and the contact initiated by her through to Peter Brorens of AgResearch New Zealand. Besides, the authors want to thank Siegbert Pachner and Daniel Grube at Ha-Co Carbon for providing the *Linum usitatissimum* fibers. Furthermore, the authors thank Tzu-Ying Chen for providing access to her institute's universal testing machine allowing the mechanical evaluation of the *L. usitatissimum* fiber samples. Moreover, the authors thank their AUT colleagues Mark Masterton for testing the *P. tenax* and carbon fiber samples, Jim Crossen for the support during the material sourcing process, and Simon Hartley for the induction to the robotics system. The authors also want to express their gratitude to Prof. Götz T. Gresser for permitting the academic secondment. Finally, the authors would like to thank the wider team, especially their fellow researchers Heiana Agnieray, Vikash Kumar, and Wuxin Yang.

Data availability

The data that support the findings of this study are openly available in the data repository of the University of Stuttgart at https://doi.org/10.18419/DARUS-5090.

References

[1] Bakis CE, Bank LC, Brown VL, Cosenza E, Davalos JF, Lesko JJ, et al. Fiber-reinforced polymer composites for construction—State-of-the-art review. J Compos Constr 2002;6(2):73–87. http://dx.doi.org/10.1061/(ASCE)1090-0268(2002)6:2(73).

[2] Gemi L, Aksoylu C, Yazman Ş, Özkılıç YO, Arslan MH. Experimental investigation of shear capacity and damage analysis of thinned end prefabricated concrete purlins strengthened by CFRP composite. Compos Struct 2019;229:111399. http://dx.doi.org/10.1016/j.compstruct.2019.111399.

[3] Chowdhury IR, Summerscales J. Woven fabrics for composite reinforcement: A review. J Compos Sci 2024;8(7). http://dx.doi.org/10.3390/jcs8070280.

[4] Spyridonos E, Witt M-U, Dippon K, Milwich M, Gresser GT, Dahy H. Natural fibre pultruded profiles: Illustration of optimisation processes to develop high-performance biocomposites for architectural and structural applications. Compos Part C: Open Access 2024;14:100492. http://dx.doi.org/10.1016/j.jcomc.2024.100492.

[5] Kobayashi S, Takada K, Nakamura R. Processing and characterization of hemp fiber textile composites with micro-braiding technique. Compos Part A: Appl Sci Manuf 2014;59:1–8. http://dx.doi.org/10.1016/j.compositesa.2013.12.009.

[6] Shrigandhi GD, Kothavale BS. Biodegradable composites for filament winding process. Mater Today: Proc 2021;42:2762–8. http://dx.doi.org/10.1016/j.matpr.2020.12.718, 3rd International Conference on Materials Engineering & Science.

[7] Lin Y, Zhu L, Chen Y, Wu K, Xiong L, Hu N. An enhanced spatial extrusion method to manufacture large-scale thermoplastic lattice structures. Addit Manuf 2024;92:104393. http://dx.doi.org/10.1016/j.addma.2024.104393.

[8] Mindermann P. Advancements in coreless filament winding towards a digital process characterization [Ph.D. thesis], University of Stuttgart; 2022, http://dx.doi.org/10.18419/opus-12622.

[9] Carosella S, Hügle S, Helber F, Middendorf P. A short review on recent advances in automated fiber placement and filament winding technologies. Compos Part B: Eng 2024;287:111843. http://dx.doi.org/10.1016/j.compositesb.2024.111843.

[10] Arrabiyeh PA, May D, Eckrich M, Dlugaj AM. An overview on current manufacturing technologies: Processing continuous rovings impregnated with thermoset resin. Polym Compos 2021;42(11):5630–55. http://dx.doi.org/10.1002/pc.26274.

[11] Ma Q, Ge J, Rejab M, Sun B, Ding Y, Nie X, et al. Fabrication of the carbon fiber reinforced plastic (CFRP) cone tube through the laboratory-scale 3-axis winding machine. Mater Today: Proc 2021;46:1645–51. http://dx.doi.org/10.1016/j.matpr.2020.07.259.

[12] Mindermann P, Gresser GT. Adaptive winding pin and hooking capacity model for coreless filament winding. J Reinf Plast Compos 2023;42(1–2):26–38. http://dx.doi.org/10.1177/07316844221094777.

[13] Mindermann P, Gresser GT. Robotic 3D deposition of impregnated carbon rovings with gradient properties for primary structures. In: Proceedings of the 69th IAC. 2018, p. C2.9.1.

[14] Duque Estrada R, Kannenberg F, Wagner HJ, Yablonina M, Menges A. Spatial winding: Cooperative heterogeneous multi-robot system for fibrous structures. Constr Robot 2020;4:205–15. http://dx.doi.org/10.1007/s41693-020-00036-7.

[15] Hildebrandt H, He M, Chen P-A, Estrada RD, Zechmeister C, et al. Slack pack: Fabrication system for the dual robotic winding of spatial fiber structures. In: Yan C, Chai H, Sun T, Yuan PF, editors. Phygital intelligence. Singapore: Springer Nature Singapore; 2024, p. 476–91. http://dx.doi.org/10.1007/978-981-99-8405-3_40.

[16] Bodea S, Mindermann P, Gresser GT, Menges A. Additive manufacturing of large coreless filament wound composite elements for building construction. 3D Print Addit Manuf 2022;9(3):145–60. http://dx.doi.org/10.1089/3dp.2020.0346.

[17] Mindermann P, Müllner R, Dieringer E, Ocker C, Klink R, Merkel M, et al. Design of fiber-composite/metal–hybrid structures made by multi-stage coreless filament winding. Appl Sci 2022;12(5):2296. http://dx.doi.org/10.3390/app12052296.

[18] Mindermann P, Witt M-U, Gresser GT. Pultrusion-winding: A novel fabrication method for coreless wound fiber-reinforced thermoset composites with distinct cross-section. Compos Part A 2022;154:106763. http://dx.doi.org/10.1016/j.compositesa.2021.106763.

[19] Minsch N, Müller M, Gereke T, Nocke A, Cherif C. Novel fully automated 3D coreless filament winding technology. J Compos Mater 2018;52(22):3001–13. http://dx.doi.org/10.1177/0021998318759743.

[20] Bodea S, Zechmeister C, Dambrosio N, Dörstelmann M, Menges A. Robotic coreless filament winding for hyperboloid tubular composite components in construction. Autom Constr 2021;126:103649. http://dx.doi.org/10.1016/j.autcon.2021.103649.

[21] Mersch J, Friese D, Le Xuan H. Toward the automation of the 3D robotic coreless filament winding process for high-performance composite materials with multiple reinforcement levels. Appl Res 2025;4(1):e202400145. http://dx.doi.org/10.1002/appl.202400145.

[22] Zechmeister C, Bodea S, Dambrosio N, Menges A. Design for long-span coreless wound, structural composite building elements. In: Gengnagel C, Baverel O, Burry J, Ramsgaard Thomsen M, Weinzierl S, editors. Impact: design with all senses. Springer International Publishing; 2020, p. 401–15.

[23] Mo Y, Ye S, Johnson S. Structural simulation, structural optimization, and winding sequence optimization strategies for the design and fabrication of coreless filament wound composite lattices. In: Advanced manufacturing of ASME international mechanical engineering congress and exposition, vol. 3, 2023, http://dx.doi.org/10.1115/IMECE2023-110952, V003T03A052.

[24] Woods BKS, Hill I, Friswell MI. Ultra-efficient wound composite truss structures. Compos Part A 2016;90:111–24. http://dx.doi.org/10.1016/j.compositesa.2016.06.022.

[25] Hunt CJ, Wisnom MR, Woods BK. WrapToR composite truss structures: Improved process and structural efficiency. Compos Struct 2019;230:111467. http://dx.doi.org/10.1016/j.compstruct.2019.111467.

[26] Xie Y, She Y, Huang J, He J, Zhou L. Experimental study on damage of steel fiber reinforced concrete- and wood-filled GFRP tubes under axial compression. Structures 2024;69:107415. http://dx.doi.org/10.1016/j.istruc.2024.107415.

[27] Azeem M, Ya HH, Alam MA, Muhammad M, M Sapuan S, Kumar M, et al. Impact response of filament-wound structure with polymeric liner: Experimental and numerical investigation (Part-A). Results Eng 2024;21:101730. http://dx.doi.org/10.1016/j.rineng.2023.101730.

[28] Gil Pérez M. Integrative structural design of non-standard building systems: coreless filament-wound structures as a case study [Ph.D. thesis], University of Stuttgart; 2023, http://dx.doi.org/10.18419/opus-12879.

[29] Gil Pérez M, Knippers J. Integrative structural design of nonstandard building systems: Bridging the gap between research and industry. Technology| Archit + Des 2023;7(2):244–61. http://dx.doi.org/10.1080/24751448.2023.2246801.

[30] Gil Pérez M, Zechmeister C, Kannenberg F, Mindermann P, Balangé L, Guo Y, et al. Computational co-design framework for coreless wound fibre-polymer composite structures. J Comput Des Eng 2022;9(2):310–29. http://dx.doi.org/10.1093/jcde/qwab081.

[31] Gil Pérez M, Mindermann P, Zechmeister C, Forster D, Guo Y, Hügle S, et al. Data processing, analysis, and evaluation methods for co-design of coreless filament-wound building systems. J Comput Des Eng 2023;10(4):1460–78. http://dx.doi.org/10.1093/jcde/qwad064.

[32] Kannenberg F, Zechmeister C, Gil Pérez M, Guo Y, Yang X, Forster D, et al. Toward reciprocal feedback between computational design, engineering, and fabrication to co-design coreless filament-wound structures. J Comput Des Eng 2024;11(3):374–94. http://dx.doi.org/10.1093/jcde/qwae048.

[33] Knippers J, Kropp C, Menges A, Sawodny O, Weiskopf D. Integrative computational design and construction: Rethinking architecture digitally. Civ Eng Des 2021;3(4):123–35. http://dx.doi.org/10.1002/cend.202100027.

[34] Dambrosio N, Zechmeister C, Pérez MG, Dörstelmann M, Stark T, Rinderspacher K, et al. Livmats pavilion: Design and development of a novel building system based on natural fibres coreless-wound structural components for applications in architecture. J Int Assoc Shell Spat Struct 2024;65(2):133–45. http://dx.doi.org/10.20898/j.iass.2024.009.

[35] Göbel M, Zechmeister C, Duque Estrada R, Weißert J, Hildebrandt H, Rossa A, et al. The hybrid flax pavilion: Towards minimally invasive bio-based Architecture – under review –. In: Sustainable built environment conference. 2025.

[36] Mindermann P, Gil Pérez M, Knippers J, Gresser GT. Investigation of the fabrication suitability, structural performance, and sustainability of natural fibers in coreless filament winding. Materials 2022;15(9):3260. http://dx.doi.org/10.3390/ma15093260.

[37] Elfaleh I, Abbassi F, Habibi M, Ahmad F, Guedri M, Nasri M, et al. A comprehensive review of natural fibers and their composites: An eco-friendly alternative to conventional materials. Results Eng 2023;19:101271. http://dx.doi.org/10.1016/j.rineng.2023.101271.

[38] Matsumoto K, Takemura K, Kitamura R, Katogi H, Tanaka T, Takagi H. Cellulose nanofiber-introduced continuous-ramie yarn-reinforced polylactic acid filament for 3D printing: Novel fabrication process and mechanical properties. Compos Part A: Appl Sci Manuf 2024;176:107836. http://dx.doi.org/10.1016/j.compositesa.2023.107836.

[39] Rust JP, Peykamian S. Yarn hairiness and the process of winding. Text Res J 1992;62(11):685–9. http://dx.doi.org/10.1177/004051759206201109.

[40] Messiry ME. Theoretical analysis of natural fiber volume fraction of reinforced composites. Alex Eng J 2013;52(3):301–6. http://dx.doi.org/10.1016/j.aej.2013.01.006.

[41] Siddiqui MS, Rabbi M, Ahmed RU, Billah MM. Biodegradable natural polymers and fibers for 3D printing: A holistic perspective on processing, characterization, and advanced applications. Clean Mater 2024;14:100275. http://dx.doi.org/10.1016/j.clema.2024.100275.

[42] Haag P, Balangé L, Di Bari R, Braun K, Weißert J, Zhang L, et al. Development of the holistic quality model and assessment – Integrating the economic quality aspect and establishing an extended interrelation analysis. Dev Built Environ 2024;19:100511. http://dx.doi.org/10.1016/j.dibe.2024.100511.

[43] Bianchi I, Prisco ND, Mancia T, Martone A, Palmieri B, Simoncini M, et al. Sustainability and economic assessment of an innovative automated filament winding process. In: Material forming. Materials research proceedings, vol. 41, Ancona, Italy: Materials Research Forum LLC; 2024, p. 2861–70. http://dx.doi.org/10.21741/9781644903131-313.

[44] University of Stuttgart. Cluster of excellence - integrative computational design and construction for architecture (IntCDC). 2024, https://www.intcdc.uni-stuttgart.de. [Accessed 16 October 2024].

[45] United Nations Environment Programme (UNEP). 2022 global status report for buildings and construction. 2022, URL https://www.unep.org/resources/publication/2022-global-status-report-buildings-and-construction.

[46] New Zealand Institute of Economic Research. The home affordability challenge - suite of policy reforms needed in New Zealand. 2014, https://www.nzier.org.nz/publications/the-home-affordability-challenge-nzier-working-paper-20144. [Accessed 12 March 2024].

[47] Ministry of Social Development. The social report 2016 – Te pūrongo oranga tangata. 2016, https://www.socialreport.msd.govt.nz/. [Accessed 12 March 2024].

[48] New Zealand Institute of Economic Research. Housing availability and affordability - A case study on the Canterbury region. 2024, https://www.nzier.org.nz/publications/housing-availability-and-affordability-nzier-insight-111. [Accessed 12 March 2024].

[49] Child Poverty Action Group. Our children, our choice: priorities for policy. 2014, https://www.cpag.org.nz/publications/our-children-our-choice-priorities-for-policy. [Accessed 12 March 2024].

[50] University of Stuttgart. Hybrid flax pavilion. 2024, https://www.icd.uni-stuttgart.de/projects/hybrid-flax-pavilion/. [Accessed 16 October 2024].

[51] Siriwardena L, Stark T, Lut S, Wagner HJ, Maierhofer M, Bechert S, et al. Joint effort - A material-robot system for fibrous joints of lightweight timber construction. In: Proceedings of the 9th ACM symposium on computational fabrication. New York, NY, USA: Association for Computing Machinery; 2024, p. 20. http://dx.doi.org/10.1145/3639473.3665791.

[52] Leder S, Kim H, Sitti M, Menges A. Enhanced co-design and evaluation of a collective robotic construction system for the assembly of large-scale in-plane timber structures. Autom Constr 2024;162:105390. http://dx.doi.org/10.1016/j.autcon.2024.105390.

[53] De Rosa IM, Santulli C, Sarasini F. Mechanical and thermal characterization of epoxy composites reinforced with random and quasi-unidirectional untreated Phormium tenax leaf fibers. Mater Des (1980- 2015) 2010;31(5):2397–405. http://dx.doi.org/10.1016/j.matdes.2009.11.059.

[54] Beg M, Pickering K, Gauss C. The effects of alkaline digestion, bleaching and ultrasonication treatment of fibre on 3D printed harakeke fibre reinforced polylactic acid composites. Compos Part A: Appl Sci Manuf 2023;166:107384. http://dx.doi.org/10.1016/j.compositesa.2022.107384.

[55] De Rosa IM, Kenny JM, Puglia D, Santulli C, Sarasini F. Tensile behavior of New Zealand flax (Phormium tenax) fibers. J Reinf Plast Compos 2010;29(23):3450–4. http://dx.doi.org/10.1177/0731684410372264.

[56] De Rosa IM, Iannoni A, Kenny J, Puglia D, Santulli C, Sarasini F, et al. Poly(lactic acid)/Phormium tenax composites: Morphology and thermo-mechanical behavior. Polym Compos 2011;32(9):1362–8. http://dx.doi.org/10.1002/pc.21159.

[57] Ramesh M. Flax (linum usitatissimum l.) fibre reinforced polymer composite materials: A review on preparation, properties and prospects. Prog Mater Sci 2019;102:109–66. http://dx.doi.org/10.1016/j.pmatsci.2018.12.004.

[58] Weston RJ, Smith GJ, Scheele SM, Williams SH. Accelerated hydrothermal degradation of fibres of Phormium tenax (New Zealand flax). J Cult Herit 2012;13(4):413–8. http://dx.doi.org/10.1016/j.culher.2011.11.006.

[59] Le Guen MJ, Newman RH. Pulped Phormium tenax leaf fibres as reinforcement for epoxy composites. Compos Part A: Appl Sci Manuf 2007;38(10):2109–15. http://dx.doi.org/10.1016/j.compositesa.2007.07.001.

[60] Te Kanawa R. Mana taonga kākahu: exploring approaches to reconnecting taonga kākahu to tangatawhenua [Ph.D. thesis], Victoria University of Wellington; 2021, http://dx.doi.org/10.26686/wgtn.17204069.v2.

[61] Wehi PM, Clarkson BD. Biological flora of New Zealand 10. Phormium tenax, harakeke, New Zealand flax. N Z J Bot 2007;45(4):521–44. http://dx.doi.org/10.1080/00288250709509737.

[62] Swarbrick N. Flax and flax working - New Zealand flax. 2007, https://www.TeAra.govt.nz/en/photograph/10377/new-zealand-flax-species. [Accessed 12 March 2024].

[63] Jones J. Alpha series issue 127 harakeke flax. 2003, https://www.royalsociety.org.nz/what-we-do/supporting-teaching-and-learning/teaching-and-learning-resources/alpha-series/. [Accessed 12 March 2024].

[64] Manaaki Whenua - Landcare Research - New Zealand's Crown Research Institute. Te kohinga harakeke o aotearoa – National New Zealand flax collection - flax cultivar uses. 2024, https://www.landcareresearch.co.nz/tools-and-resources/collections/new-zealand-flax-collections/flax-cultivar-uses/. [Accessed 12 March 2024].

[65] Alexander-Maaka K. Te kāuru hou—a new leaf: processing harakeke (phormium tenax) for wholeGarment knitting technology - shima seiki [Ph.D. thesis], Auckland University of Technology School of Art and Design; 2019.

[66] Newman R. Harakeke: Traditional and new uses. In: Proceedings of the biopolymer network: creating a focus of scientific and technological excellence in the conversion of sustainable natural resources to biopolymers and biocomposites. SCION; 2007, p. 1–27.

[67] Tan LM. Harakeke fibre as reinforcement in epoxy matrix composites and its hybridisation with hemp fibre [Ph.D. thesis], The University of Waikato; 2016.

[68] Le Guen MJ. New Zealand flax fibre potential as composite reinforcement. In: Proceedings of the KBBE workshop, boucherville, 1st August 2013. 2013, p. 1–18.

[69] Yeturu Farms. Introduction to agave sisal fibre. 2025, URL https://yeturufarms.com/sisal-fibre/. [Accessed 12 March 2025].

[70] KiwiFibre Innovations Ltd. KiwiFibre - our growers - why harakeke. 2024, https://www.kiwifibre.com/growers-1. [Accessed 12 September 2024].

[71] Brorens PH, Newman RH, Le Guen MJ, Barker RHT, Taylor ME. Restoring New Zealand's harakeke fibre industry. In: Natural fibres in australasia, proceedings of the combined (NZ and AUS) conference of the textile institute, dunedin 15-17 april. 2009, p. 97–102.

[72] Le Guen MJ, Newman R, Fernyhough A, Hill S, Staiger M. Correlations between the physiochemical characteristics of plant fibres and their mechanical properties. In: Natural fibres: advances in science and technology towards industrial applications, vol. 12, Springer; 2016, p. 35–47.

[73] Carr D, Cruthers N, Smith C, Myers T. Identification of selected vegetable textile fibres. Stud Conserv 2008;53(sup2):75–87. http://dx.doi.org/10.1179/sic.2008.53.Supplement-2.75.

[74] Newman RH, Le Guen MJ, Battley MA, Carpenter JE. Failure mechanisms in composites reinforced with unidirectional Phormium leaf fibre. Compos Part A: Appl Sci Manuf 2010;41(3):353–9. http://dx.doi.org/10.1016/j.compositesa.2009.11.001.

[75] Kane F, Brorens P, Guen MJL, Kilford A, Ruka T. Exploring a place-based approach to materials design: Harakeke nonwovens in Aotearoa New Zealand. 2019, http://dx.doi.org/10.17028/rd.lboro.9724661.v1, Loughborough University.

[76] Furtado F, Sydenstricker Flores-Sahagun T, Szlapak Franco T. Analysis of polymeric composites of Phormium tenax. Biointerface Res Appl Chem 2023;13:124. http://dx.doi.org/10.33263/BRIAC132.124.

[77] Wypych F, Pereira Ramos L, Satyanarayana K. Comparative study of Brazilian natural fibers and their composites with others. In: Handbook of engineering biopolymers. Hanser; 2007, p. 473–522.

[78] Mahir FI, Keya KN, Sarker B, Nahiun KM, Khan RA. A brief review on natural fiber used as a replacement of synthetic fiber in polymer composites. Mater Eng Res 2019;1:86–97. http://dx.doi.org/10.25082/MER.2019.02.007.

[79] Abbel R, Risani R, Nourtier M, Donaldson L, Brunschwig C, Mayer-Laigle C, et al. Coating of hemp fibres with hydrophobic compounds extracted from pine bark. Fibers 2024;12:96. http://dx.doi.org/10.3390/fib12110096.

[80] Ding J, Liang L, Meng X, Yang F, Pu Y, Ragauskas AJ, et al. The physiochemical alteration of flax fibers structuring components after different scouring and bleaching treatments. Ind Crop Prod 2021;160:113112. http://dx.doi.org/10.1016/j.indcrop.2020.113112.

[81] Li Y, Mai Y-W, Ye L. Sisal fibre and its composites: a review of recent developments. Compos Sci Technol 2000;60:2037–55. http://dx.doi.org/10.1016/S0266-3538(00)00101-9.

[82] Kadivar M, Gauss C, Mármol G, de Sá AD, Fioroni C, Ghavami K, et al. The influence of the initial moisture content on densification process of D. asper bamboo: Physical-chemical and bending characterization. Constr Build Mater 2019;229:116896. http://dx.doi.org/10.1016/j.conbuildmat.2019.116896.

[83] Hartono R, Iswanto AH, Priadi T, Herawati E, Farizky F, Sutiawan J, et al. Physical, chemical, and mechanical properties of six bamboo from Sumatera Island Indonesia and its potential applications for composite materials. Polymers 2022;14:4868. http://dx.doi.org/10.3390/polym14224868.

[84] Hu K, Huang Y, Fei B, Yao C, Zhao C. Investigation of the multilayered structure and microfibril angle of different types of bamboo cell walls at the micro/nano level using a LC-PolScope imaging system. Cellulose 2017;24:4611–25. http://dx.doi.org/10.1007/s10570-017-1447-y.

[85] Richter S, Müssig J, Gierlinger N. Functional plant cell wall design revealed by the Raman imaging approach. Planta 2011;233:763–72. http://dx.doi.org/10.1007/s00425-010-1338-z.

[86] Bachmann J, Hidalgo C, Bricout S. Environmental analysis of innovative sustainable composites with potential use in aviation sector—A life cycle assessment review. Sci China Technol Sci 2017;60:1301–17. http://dx.doi.org/10.1007/s11431-016-9094-y.

[87] Di Giorgio L, Salgado P, Dufresne A, Mauri A. Nanocelluloses from phormium (Phormium tenax) fibers. Cellulose 2020;27:4975–90. http://dx.doi.org/10.1007/s10570-020-03120-x.

[88] Fortunati E, Puglia D, Monti M, Peponi L, Santulli C, Kenny J, et al. Extraction of cellulose nanocrystals from Phormium tenax fibres. J Polym Environ 2012;21:319–28. http://dx.doi.org/10.1007/s10924-012-0543-1.

[89] Amiandamhen S, Meincken M, Tyhoda L. Natural fibre modification and its influence on fibre-matrix interfacial properties in biocomposite materials. Fibers Polym 2020;21. http://dx.doi.org/10.1007/s12221-020-9362-5.

[90] Manian AP, Cordin M, Pham T. Extraction of cellulose fibers from flax and hemp: a review. Cellulose 2021;28:8275–94. http://dx.doi.org/10.1007/s10570-021-04051-x.

[91] Komuraiah A, Kumar N, Prasad B. Chemical composition of natural fibers and its influence on their mechanical properties. Mech Compos Mater 2014;50:359–76. http://dx.doi.org/10.1007/s11029-014-9422-2.

[92] Lowe B, Carr DJ, McCallum RE, Myers T, Niven BE, Cameron R, et al. Identifying harakeke (Phormium tenax) cultivars using whītau and fibre aggregate properties. In: Wilson CA, Laing RM, editors. Natural fibres in australasia: proceedings of the combined (NZ and AUS) conference of the textile institute. Dunedin, New Zealand: The Textile Institute; 2009, p. 121–5.

[93] Museum of New Zealand - Te Papa Tongarewa. Muka - flax fibre. 2018, https://collections.tepapa.govt.nz/topic/3626#:~:text=Extracting%20and%20processing%20muka,soften%20the%20threads%20for%20weaving. [Accessed 12 September 2024].

[94] Carr DJ, Cruthers NM, Laing RM, Niven BE. Fibers from three cultivars of New Zealand flax (Phormium tenax). Text Res J 2005;75(2):93–8. http://dx.doi.org/10.1177/004051750507500201.

[95] Cruthers NM, Carr DJ, Laing RM, Niven BE. Structural differences among fibers from six cultivars of harakeke (Phormium tenax, New Zealand flax). Text Res J 2006;76(8):601–6. http://dx.doi.org/10.1177/0040517506065603.

[96] Museum of New Zealand - Te Papa Tongarewa. Harakeke - New Zealand flax. 2018, https://collections.tepapa.govt.nz/topic/3623. [Accessed 15 March 2025].

[97] Natasha Cruthers DC, Laing R. The New Zealand flax fibre industry. Text Hist 2009;40(1):103–11. http://dx.doi.org/10.1179/174329509x452577.
[98] Mindermann P, Rongen B, Gubetini D, Knippers J, Gresser GT. Material monitoring of a composite dome pavilion made by robotic coreless filament winding. Materials 2021;14(19). http://dx.doi.org/10.3390/ma14195509.
[99] Teijin. Tenax filament yarn - product data sheet. 2024, https://www.teijincarbon.com/fileadmin/user_upload/Datenbl¨atter/Filament_Yarn/Product_Data_Sheet_TSG01en_EU_Filament_.pdf. [Accessed 12 September 2024-09-12].
[100] Aruan Efendy M, Pickering K. Comparison of harakeke with hemp fibre as a potential reinforcement in composites. Compos Part A: Appl Sci Manuf 2014;67:259–67. http://dx.doi.org/10.1016/j.compositesa.2014.08.023.
[101] Newman RH, Clauss EC, Carpenter JE, Thumm A. Epoxy composites reinforced with deacetylated Phormium tenax leaf fibres. Compos Part A: Appl Sci Manuf 2007;38(10):2164–70. http://dx.doi.org/10.1016/j.compositesa.2007.06.007.
[102] Corrales F, Vilaseca F, Llop M, Gironès J, Méndez J, Mutjè P. Chemical modification of jute fibers for the production of green-composites. J Hazard Mater 2007;144(3):730–5. http://dx.doi.org/10.1016/j.jhazmat.2007.01.103.
[103] Li X, Tabil LG, Panigrahi S. Chemical treatments of natural fiber for use in natural fiber-reinforced composites: A review. J Polym Environ 2007;15(1):25–33. http://dx.doi.org/10.1007/s10924-006-0042-3.
[104] Savastano H, Santos S, Fiorelli J, Agopyan V. 19 - sustainable use of vegetable fibres and particles in civil construction. In: Khatib JM, editor. Sustainability of construction materials. 2nd ed.. Woodhead Publishing; 2016, p. 477–520. http://dx.doi.org/10.1016/B978-0-08-100370-1.00019-6.
[105] Khan T, Sultan MTBH, Ariffin AH. The challenges of natural fiber in manufacturing, material selection, and technology application: A review. J Reinf Plast Compos 2018;37(11):770–9. http://dx.doi.org/10.1177/0731684418756762.
[106] Broeren ML, Dellaert SN, Cok B, Patel MK, Worrell E, Shen L. Life cycle assessment of sisal fibre – Exploring how local practices can influence environmental performance. J Clean Prod 2017;149:818–27. http://dx.doi.org/10.1016/j.jclepro.2017.02.073.
[107] Dicker MP, Duckworth PF, Baker AB, Francois G, Hazzard MK, Weaver PM. Green composites: A review of material attributes and complementary applications. Compos Part A: Appl Sci Manuf 2014;56:280–9. http://dx.doi.org/10.1016/j.compositesa.2013.10.014.
[108] Terre de Lin. Terre de lin. 2024, https://www.terredelin.com/HP/HPInternet_uk.aspx. [Accessed 16 October 2024].
[109] Adhesive Technologies NZLTD. ADR246. 2024, https://adhesivetechnologies.co.nz/laminating-infusion-and-pre-pref-resins/adr246/. [Accessed 12 September 2024].
[110] Iwano Y, Wada A, Takayama R, Tanaka M, Zhou Y, Ohashi I, et al. Design and fabrication of an automotive frame model leveraging anisotropic topology optimization and tailored fiber placement. Mech Eng J 2024;11(2):1–13. http://dx.doi.org/10.1299/mej.24-00008.
[111] Gil Pérez M. Structural design challenges of bio-based composites and digital fabrication towards sustainable building systems. In: Block P, Boller G, DeWolf C, Pauli J, Kaufmann W, editors. Redefining the Art of Structural Design, Proceedings of the IASS 2024 Symposium. 2024, p. 153.
[112] Mindermann P, Kaiser P, Müller L, Fischer L, Gebhardt P, Hindenlang U, et al. Investigation of different load transmission concepts for coreless filament wound structures. Compos Struct 2023;303:116287. http://dx.doi.org/10.1016/j.compstruct.2022.116287.
[113] Gil Pérez M, Dambrosio N, Rongen B, Menges A, Knippers J. Structural optimization of coreless filament wound components connection system through orientation of anchor points in the winding frames. In: IASS annual symposium. Barcelona, Spain; 2019, p. 1381–8.
[114] Mindermann P, Gil Pérez M, Kamimura N, Knippers J, Gresser GT. Implementation of fiber-optical sensors into coreless filament-wound composite structures. Compos Struct 2022;290:115558. http://dx.doi.org/10.1016/j.compstruct.2022.115558.
[115] Mindermann P, Witt M-U, Samie A, Selvarayan SK, Gresser GT. Integration of ceramic matrix systems into coreless filament wound fiber-reinforced composite lightweight structures for lunar resource utilization. Compos Part C: Open Access 2024;15:100508. http://dx.doi.org/10.1016/j.jcomc.2024.100508.
[116] Mindermann P, Acker D, Wegner R, Fasoulas S, Gresser GT. Long-span fiber composite truss made by coreless filament winding for large-scale satellite structural systems demonstrated on a planetary sunshade concept. Sci Rep 2024;14:8190. http://dx.doi.org/10.1038/s41598-024-58513-w.
[117] Hunt CJ, Zhao Y, Wisnom MR, Woods BK. WrapToR composite truss structures: Measurement and modelling of mechanical response. Compos Struct 2020;254:112834. http://dx.doi.org/10.1016/j.compstruct.2020.112834.
[118] Mindermann P, Bodea S, Menges A, Gresser GT. Development of an impregnation end-effector with fiber tension monitoring for robotic coreless filament winding. Processes 2021;9(5):806. http://dx.doi.org/10.3390/pr9050806.
[119] ABB. Produktspezifikation IRB 2600. 2024, https://library.e.abb.com/public/5326a234fe07466f8d510f595348cf9a/3HAC035959%20PS%20IRB%202600%20on%20IRC5-de.pdf. [Accessed 16 October 2024].
[120] Nogueira P, Ramírez C, Torres A, Abad MJ, Cano J, López J, et al. Effect of water sorption on the structure and mechanical properties of an epoxy resin system. J Appl Polym Sci 2001;80:71–80. http://dx.doi.org/10.1002/1097-4628(20010404)80:1<71::AID-APP1077>3.0.CO;2-H.
[121] Gil Pérez M, Guo Y, Knippers J. Integrative material and structural design methods for natural fibres filament-wound composite structures: The LivMatS pavilion. Mater Des 2022;217:110624. http://dx.doi.org/10.1016/j.matdes.2022.110624.
[122] RS PRO. RS PRO white rubber sponge sheet, 600mm x 600mm x 1.5mm. 2022, https://docs.rs-online.com/2cd8/A700000008880291.pdf. [Accessed 9 October 2024].
[123] Saadati Y, Chatelain J-F, Lebrun G, Beauchamp Y, Bocher P, Vanderesse N. A study of the interlaminar fracture toughness of unidirectional flax/epoxy composites. J Compos Sci 2020;4(2):66. http://dx.doi.org/10.3390/jcs4020066.
[124] Cáceres GdA, Lisbôa TdV, Elschner C, Spickenheuer A. Experimental global warming potential-weighted specific stiffness comparison among different natural and synthetic fibers in a composite component manufactured by tailored fiber placement. Polymers 2024;16:726. http://dx.doi.org/10.3390/polym16060726.
[125] Shah DU. Developing plant fibre composites for structural applications by optimising composite parameters: a critical review. J Mater Sci 2013;48(18):6083–107. http://dx.doi.org/10.1007/s10853-013-7458-7.
[126] Duchemin B, Luijk KV, Staiger M. New Zealand flax (Phormium tenax) reinforced eco-composites. In: EcoComp, 2nd international conference on composites. 2003, p. 1–6.
[127] Johlitz M. Zum Alterungsverhalten von Polymeren: experimentell gestützte, thermo-chemomechanische Modellbildung und numerische Simulation [Ph.D. thesis], University of the Bundeswehr Munich; 2015, URL https://www.unibw.de/lrt4/personen/johlitz-2015-groesse_reduziert.pdf.
[128] Altair. Employing simulation-driven solutions to develop an iconic sculpture. 2025, https://altair.com/te-ahi-tupua-hemo-gorge-sculpture. [Accessed 15 March 2025].